Journal of Computational Physics 228 (2009) 4714–4744

Contents lists available at ScienceDirect

Journal of Computational Physics

journal homepage: www.elsevier.com/locate/jcp

A conservative discrete compatibility-constraint low-Mach pressure-correction algorithm for time-accurate simulations of variable density flows

Pieter Rauwoens *, Jan Vierendeels, Erik Dick, Bart Merci

Ghent University – UGent, Dept. of Flow, Heat and Combustion Mechanics, Sint-Pietersnieuwstraat 41, B-9000 Ghent, Belgium

ARTICLE INFO

Article history:
Received 11 April 2008
Received in revised form 17 March 2009
Accepted 19 March 2009
Available online 5 April 2009

MSC:
65N12
65N22
76D05
76M12
76R99

Keywords:
Low-Mach
Pressure-correction
Variable density flow
Mass conservation
Stability
Equation of state

ABSTRACT

In this paper, we develop the discrete compatibility-constraint pressure-correction algorithm for transient simulations of variable density flows at low-Mach numbers. The constraint for the velocity field is constructed from a combination of the discrete equations of continuity and scalar (e.g. energy) transport, imposing that the newly predicted state must be compatible, in agreement with the equation of state. This way, mass and scalar conservation are guaranteed and the equation of state is exactly fulfilled at every time step. For comparison reasons, two other types of well-known pressure-correction algorithms are also used. The first class, denoted as continuity-constraint pressure-correction, is based on a constraint for the velocity field that is derived solely from the continuity equation. The second class, denoted as analytical compatibility-constraint pressure-correction, constructs the constraint from an analytical combination of the material derivative of the equation of state and the continuity and scalar equations. The algorithms are tested for three example fluid configurations: a single-fluid ideal gas, a two-fluid inert mixture and a two-fluid reacting mixture. The latter is special in the sense that the equation of state is non-linear and not everywhere differentiable. The continuity-constraint pressure-correction algorithm yields unstable solutions if density ratios are high. The analytical compatibility-constraint pressure-correction algorithm yields stable results, but the predicted states do not correspond to the equation of state. The discrete compatibility-constraint pressure-correction algorithm performs well on all test cases: the simulation results are stable and exactly match the equation of state.

1. Introduction

Various flow regimes in industrial devices are of low speed nature. Such flows are called *incompressible*, since the velocities are much smaller than the speed of sound. In non-reacting incompressible flows without heat transfer, the use of a pressure-correction algorithm has proven to be accurate and efficient (e.g. [3,4]). Since density remains constant, no substantial problems are encountered and the solution is straightforward. The mass conservation equation naturally imposes a constraint on the velocity field, so that a solenoidal velocity field is obtained. No instabilities are observed in a segregated solution procedure when the convective CFL stability condition for the time step is respected. However, if density varies strongly

* Corresponding author.
E-mail addresses: Pieter.Rauwoens@UGent.be (P. Rauwoens), Jan.Vierendeels@UGent.be (J. Vierendeels), Erik.Dick@UGent.be (E. Dick), Bart.Merci@UGent.be (B. Merci).

0021-9991/$ - see front matter © 2009 Elsevier Inc. All rights reserved.
doi:10.1016/j.jcp.2009.03.036

in time and space, e.g. due to temperature variation, the set of equations becomes more coupled and an efficient solution is no longer obvious. Various attempts have been made to create efficient solution methods.

A basic difficulty stems from the acoustic waves in the compressible formulation. As acoustic waves act at a substantially smaller time scale than the convective phenomena in low Mach number flows, the acoustic modes do not significantly influence the solution and may be regarded as superfluous. The use of larger time steps, corresponding to the convective scales, can therefore strongly improve computational efficiency without loss of relevant information. Larger time steps can be obtained by using implicit methods. To increase efficiency, convective terms can be treated explicitly, while only acoustic terms and viscous terms, which form linear operators, are treated implicitly [22]. An alternative is to reduce the acoustic time step limit by preconditioning techniques [19,25]. Since, however, time accuracy has to be respected for convective phenomena, care has to be taken in the construction of the preconditioning [24]. Implicit methods or explicit methods with preconditioning essentially are meant to be all-Mach techniques, which means that they also allow accurate solutions for higher Mach numbers.

Here, for efficiency reasons, we take the choice to formulate the equations in the low-Mach number form. In these equations, the acoustic phenomena are eliminated. The pressure is split into a thermodynamic and a hydrodynamic part. As for constant density flow, the hydrodynamic pressure has to be treated implicitly in order to obtain stability. Solution of the equations in coupled form is possible, but full coupling of all the variables is not necessary. As for constant density flow, only pressure–velocity coupling is needed. So, the most obvious technique is to solve the equations in a segregated way, using a pressure-correction algorithm.

Many algorithms, although performing well for constant density (non-reacting) flows, give rise to instabilities in flows, where the density can vary strongly from cell to cell [15,21]. These algorithms belong to the class denoted here as *continuity-constraint pressure-correction schemes*. Other algorithms perform better with respect to stability, but generate solutions that satisfy the equation of state only in an approximate manner [6,21]. These algorithms are denoted here as *analytical compatibility-constraint pressure-correction schemes*. Because of these shortcomings, we develop an algorithm that (i) is stable and robust, (ii) conserves mass and scalars (such as energy and fuel elements mass), (iii) predicts states that satisfy the equation of state in an exact manner and (iv) allows time-accurate solutions. We call this new algorithm the *discrete compatibility-constraint pressure-correction scheme*.

In the paper, the three different pressure-correction algorithms are investigated by means of a set of one-dimensional test cases, involving convection and diffusion of sharp initial scalar gradients. In these test-cases, three fluid configurations are investigated: a single-fluid ideal gas at different temperatures, a two-fluid non-reacting flow and a two-fluid combusting flow. We consider the 1D test problem as a necessary condition for a scheme to yield stable solutions in a general variable-density problem. After describing the equations in low-Mach number formulation, the equations of state for the three types of fluids are presented. After the description of the three pressure-correction schemes, the results for the 1D test cases of purely convective and conductive transport, are reported and discussed. From these results, we conclude that only the discrete compatibility-constraint pressure-correction scheme yields stable results in all cases, specifically for a non-linear and/or non-differentiable equation of state, providing a stable and consistent mass-conserving algorithm. Finally, these findings are confirmed by the two-dimensional test cases of a non-reacting and reacting mixing layer and a transient flame calculation.

2. Governing equations

2.1. Low Mach number equations for single fluid ideal gas flow

With the summation convention, the set of equations for non-reacting flows, expressing conservation of mass, momentum and energy, reads:

$$\frac{\partial \hat{\rho}}{\partial \hat{t}} + \frac{\partial(\hat{\rho}\hat{u}_i)}{\partial \hat{x}_i} = 0, \tag{1}$$

$$\frac{\partial(\hat{\rho}\hat{u}_j)}{\partial \hat{t}} + \frac{\partial(\hat{\rho}\hat{u}_i\hat{u}_j)}{\partial \hat{x}_i} = -\frac{\partial \hat{p}}{\partial \hat{x}_j} + \frac{\partial \hat{\tau}_{ij}}{\partial \hat{x}_i} + \hat{\rho}\hat{g}\delta_{j3}, \tag{2}$$

$$\frac{\partial(\hat{\rho}\hat{E})}{\partial \hat{t}} + \frac{\partial(\hat{\rho}\hat{u}_i\hat{H})}{\partial \hat{x}_i} = \frac{\partial(\hat{\tau}_{ij}\hat{u}_j)}{\partial \hat{x}_i} + \frac{\partial}{\partial \hat{x}_i}\left(\hat{\kappa}\frac{\partial \widehat{T}}{\partial \hat{x}_i}\right) + \hat{\rho}\hat{g}\hat{u}_3 \tag{3}$$

with $\hat{\tau}_{ij} = \hat{\mu}\left[\left(\frac{\partial \hat{u}_i}{\partial \hat{x}_j} + \frac{\partial \hat{u}_j}{\partial \hat{x}_i}\right) - \frac{2}{3}\frac{\partial \hat{u}_k}{\partial \hat{x}_k}\delta_{ij}\right]$. The $\hat{}$-notation is used to indicate dimensional variables. Without lack of generality, we assume that gravity is aligned with the third axis, pointing downwards. The total energy and total enthalpy per unit mass are given by the relations $\widehat{E} = \hat{e} + \frac{1}{2}|\hat{u}|^2$ and $\widehat{H} = \widehat{E} + \frac{\hat{p}}{\hat{\rho}}$. We also assume a perfect and ideal gas, with equation of state and caloric equation:

$$\hat{p} = \hat{\rho}\widehat{R}\widehat{T}, \quad \hat{e} = \hat{c_v}\hat{T}. \tag{4}$$

Introducing the non-dimensional variables:

$$\rho = \frac{\hat{\rho}}{\hat{\rho}_\infty}, \quad p = \frac{\hat{p}}{\hat{p}_\infty}, \quad u_j = \frac{\hat{u}_j}{\hat{u}_\infty}, \quad T = \frac{\widehat{T}}{\hat{p}_\infty/\widehat{R}\hat{\rho}_\infty}, \quad \mu = \frac{\hat{\mu}}{\hat{\mu}_\infty}, \quad \kappa = \frac{\hat{\kappa}}{\hat{\kappa}_\infty},$$
$$x_j = \frac{\hat{x}_j}{\widehat{L}}, \quad t = \frac{\hat{t}}{\widehat{L}/\hat{u}_\infty}, \quad E = \frac{\widehat{E}}{\hat{p}_\infty/\hat{\rho}_\infty}, \quad H = \frac{\widehat{H}}{\hat{p}_\infty/\hat{\rho}_\infty}, \tag{5}$$

five non-dimensional parameters appear (with $\widetilde{M} = M\sqrt{\gamma}$):

$$\widetilde{M}_\infty = \frac{\hat{u}_\infty}{\sqrt{\hat{p}_\infty/\hat{\rho}_\infty}}, \quad Re_\infty = \frac{\hat{\rho}_\infty \hat{u}_\infty \widehat{L}}{\hat{\mu}_\infty}, \quad Fr_\infty = \frac{\hat{u}_\infty}{\sqrt{\hat{g}\widehat{L}}}, \quad Pr_\infty = \frac{\hat{c}_p \hat{\mu}_\infty}{\hat{\kappa}_\infty}, \quad \gamma = \frac{\hat{c}_p}{\hat{c}_v} \tag{6}$$

and the non-dimensional Navier–Stokes equations become:

$$\frac{\partial \rho}{\partial t} + \frac{\partial(\rho u_i)}{\partial x_i} = 0, \tag{7}$$
$$\frac{\partial(\rho u_j)}{\partial t} + \frac{\partial(\rho u_i u_j)}{\partial x_i} = -\frac{1}{\widetilde{M}_\infty^2}\frac{\partial p}{\partial x_j} + \frac{1}{Re_\infty}\frac{\partial \tau_{ij}}{\partial x_i} + \frac{1}{Fr_\infty^2}\rho\delta_{j3}, \tag{8}$$
$$\frac{\partial(\rho E)}{\partial t} + \frac{\partial(\rho u_i H)}{\partial x_i} = \frac{\widetilde{M}_\infty^2}{Re_\infty}\frac{\partial(\tau_{ij}u_j)}{\partial x_i} + \frac{\gamma}{(\gamma-1)Re_\infty Pr_\infty}\frac{\partial}{\partial x_i}\left(\kappa\frac{\partial T}{\partial x_i}\right) + \frac{\widetilde{M}_\infty^2}{Fr_\infty^2}\rho u_3. \tag{9}$$

The total energy and total enthalpy are now given by $E = e + \widetilde{M}_\infty^2 \frac{1}{2}|u|^2, H = E + \frac{p}{\rho}$. The non-dimensional state and caloric equations become

$$p = \rho T, \quad e = \frac{1}{\gamma - 1}T. \tag{10}$$

Restricting ourselves to low Mach number flows, the set of Eqs. (7)–(9) can be simplified. Each variable is expanded into a power series of $\widetilde{M}_\infty$ and the asymptotic limit, $\widetilde{M}_\infty$ going to zero, is taken. For each variable, the lowest order term remains in the equations, except for the pressure, which consists of two parts: a thermodynamic part $p_0 (= \rho T)$ and a hydrodynamic part p_2:

$$p = p_0 + \widetilde{M}_\infty^2 p_2. \tag{11}$$

The low-Mach number equations, with the energy equation formulated in terms of temperature, read [8,9,12]:

$$p_0 = p_0(t), \tag{12}$$
$$\frac{\partial \rho}{\partial t} + \frac{\partial(\rho u_i)}{\partial x_i} = 0, \tag{13}$$
$$\frac{\partial(\rho u_j)}{\partial t} + \frac{\partial(\rho u_i u_j)}{\partial x_i} = -\frac{\partial p_2}{\partial x_j} + \frac{1}{Re_\infty}\frac{\partial \tau_{ij}}{\partial x_i} + \frac{1}{Fr_\infty^2}\rho\delta_{j3}, \tag{14}$$
$$\frac{\gamma}{\gamma-1}\rho\left[\frac{\partial T}{\partial t} + u_i\frac{\partial T}{\partial x_i}\right] - \frac{dp_0}{dt} = \frac{\gamma}{(\gamma-1)Re_\infty Pr_\infty}\frac{\partial}{\partial x_i}\left(\kappa\frac{\partial T}{\partial x_i}\right). \tag{15}$$

with the equation of state

$$p_0 = \rho T. \tag{16}$$

By combination of (13) and (15), the equation for temperature can be reformulated in conservative form. With (16), the result is

$$\frac{dp_0}{dt} + \gamma p_0 \frac{\partial u_i}{\partial x_i} = \frac{\gamma}{Re_\infty Pr_\infty}\frac{\partial}{\partial x_i}\left(\kappa\frac{\partial T}{\partial x_i}\right). \tag{17}$$

So, for ideal gas, the energy equation leads to a constraint on the divergence of the velocity field. In open systems, the thermodynamic pressure p_0 is assumed constant in space and time, so that the constraint (17) simplifies further.

Note that for low-Mach number flows, the combination of the continuity Eq. (7) and the energy Eq. (9), always leads to a constraint on the divergence of the velocity field, whatever the equation of state is. Indeed, in the limit for $\widetilde{M}_\infty \to 0$, the kinetic energy contributions in E and H dissapear. Through the equation of state and the caloric equation, density and energy per unit volume are given by

$$\rho = \rho(p_0, T), \quad \rho e = \rho e(p_0, T). \tag{18}$$

The continuity equation (7) and energy equation (9) can be written in advective form, which read, for low Mach number flow:

$$\frac{\partial \rho}{\partial t} + u_i\frac{\partial \rho}{\partial x_i} = -\rho\frac{\partial u_i}{\partial x_i}, \tag{19}$$
$$\frac{\partial \rho e}{\partial t} + u_i\frac{\partial(\rho e)}{\partial x_i} = -\rho e\frac{\partial u_i}{\partial x_i} - p_0\frac{\partial u_i}{\partial x_i} + Cond(T), \tag{20}$$

where *Cond* is the conduction term in the energy equation (15). By expanding ρ as function of p_0 and T in the left hand side of (19) and by expanding ρe as function of p_0 and T in the left hand side of (20) and making the combination that eliminates T from the left hand side, a constraint on the divergence of the velocity is obtained. For the special case of an ideal gas, the energy equation itself forms the constraint, since ρe is proportional to p_0 and is independent of T, leading to (17).

From now on, we call the constraining equation for the divergence of the velocity field as a result of a combination of the continuity and the energy equation, the compatibility constraint. The meaning of the term is that for low-Mach number flow, both the continuity equation and the energy equation determine p_0 and T, and that the results of both equations have to be compatible with each other. Since, at low Mach numbers, the thermodynamic pressure is uniform in space, and can be calculated a priori, only the temperature remains as unknown value. As a result, the two equations have to determine the same temperature field, putting a constraint on the divergence of the velocity field.

2.2. Mixture fraction equation for two fluid flows

For combusting flows, the general non-dimensional species transport equations read:

$$\frac{\partial(\rho Y_l)}{\partial t}+\frac{\partial(\rho u_i Y_l)}{\partial x_i}=\frac{1}{Re_\infty Pr_\infty Le_\infty}\frac{\partial}{\partial x_i}(J_{li})+\dot{\omega}_l, \tag{21}$$

with

$$Le_\infty=\frac{\hat{\kappa}_\infty}{\hat{\rho}_\infty \hat{D}_\infty \hat{c}_p}. \tag{22}$$

Assuming Fick's diffusion law with equal diffusivities for all species and neglecting the Soret-effect, these equations can be lumped into one equation for the mixture fraction ξ (e.g. [10]):

$$\frac{\partial(\rho\xi)}{\partial t}+\frac{\partial(\rho u_i\xi)}{\partial x_i}=\frac{1}{Re_\infty Pr_\infty Le_\infty}\frac{\partial}{\partial x_i}\left(\rho D\frac{\partial\xi}{\partial x_i}\right). \tag{23}$$

The mixture fraction is a non-dimensional normalized variable, with $\xi=0$ in pure air and $\xi=1$ in pure fuel. Eq. (23) does not contain a chemical source term. From ξ, the species mass fractions are obtained with a chemistry model. Furthermore, in the absence of radiation ('adiabatic circumstances'), and if unity Lewis number ($Le=\hat{\kappa}/(\hat{\rho}\hat{D}\hat{c}_p)=1$) is considered for all species, the normalized static enthalpy variable ($(h-h_O)/(h_F-h_O)$), obeys the same transport equation (23) with the same boundary and initial conditions (e.g. [10]). Hence, no additional transport equation for static enthalpy is solved. The static enthalpy consists of the chemical formation enthalpy and the sensible enthalpy. The contribution of each individual term depends on the chemistry model. Thus, temperature follows from ξ through the chemistry model and no energy transport equation in terms of temperature is solved in such circumstances. So, the mixture fraction equation replaces the energy equation and the equation of state is given as

$$\rho=\rho(p_0,\xi). \tag{24}$$

On physical grounds, to preserve conservation properties, the equation of state is formulated as

$$\rho=\rho(p_0,\rho\xi). \tag{25}$$

Remark that the equation of state (24) or (25) for reacting flows generally is non-linear and not everywhere differentiable, as we illustrate later. So, it is quite challenging to develop a method that allows such an equation of state.

Combination of the continuity equation (7) and the mixture fraction equation (23), leads to a compatibility constraint for the divergence of the velocity field. We introduce the quantity fuel elements density (literally: the amount of mass of the chemical elements, originating from the fuel inlet, per unit of volume) $f=\rho\xi$ and write the equation of state as $\rho=\mathcal{H}_C(f)$. So, we assume that the thermodynamic pressure is constant. The notation $\mathcal{H}_C$ refers to the fact that the chemistry model determines the relation between f and ρ. The mixture fraction equation then becomes:

$$\frac{\partial f}{\partial t}+\frac{\partial(f u_i)}{\partial x_i}=\frac{1}{Re_\infty Pr_\infty Le_\infty}\frac{\partial}{\partial x_i}\left(\rho D\frac{\partial\xi}{\partial x_i}\right). \tag{26}$$

We expand as:

$$\frac{\mathrm{d}f}{\mathrm{d}\rho}\left(\frac{\partial\rho}{\partial t}+u_i\frac{\partial\rho}{\partial x_i}\right)+f\frac{\partial u_i}{\partial x_i}=Diff(\xi), \tag{27}$$

where *Diff* means the diffusive term in (26). Elimination of the material derivative of density between Eqs. (19) and (27) leads to the compatibility equation:

$$\left(f-\rho\frac{\mathrm{d}f}{\mathrm{d}\rho}\right)\frac{\partial u_i}{\partial x_i}=Diff(\xi). \tag{28}$$

It is clear that the compatibility equation is only well defined when f is everywhere differentiable. In practice, this is not always the case, as will be illustrated later.

A further problem, concerning conservation properties, occurs when f is a non-linear function of ρ. To illustrate this problem, we try to recombine the conservative mixture fraction equation (26) and the constraint (28), to obtain the continuity equation (13). The constraint (28) is written as:

$$\frac{\partial(fu_i)}{\partial x_i} = u_i \frac{\partial}{\partial x_i}\left[f - \rho\frac{\mathrm{d}f}{\mathrm{d}\rho}\right] + \frac{\partial}{\partial x_i}\left(\frac{\mathrm{d}f}{\mathrm{d}\rho}\rho u_i\right) + Diff(\xi) \tag{29}$$

and filled out in the mixture fraction equation (26):

$$\frac{\partial f}{\partial t} + u_i \frac{\partial}{\partial x_i}\left[f - \rho\frac{\mathrm{d}f}{\mathrm{d}\rho}\right] + \frac{\partial}{\partial x_i}\left(\frac{\mathrm{d}f}{\mathrm{d}\rho}\rho u_i\right) = 0. \tag{30}$$

The time derivative of f can be replaced by a density time derivative

$$\frac{\mathrm{d}f}{\mathrm{d}\rho}\frac{\partial\rho}{\partial t} + u_i \frac{\partial}{\partial x_i}\left[f - \rho\frac{\mathrm{d}f}{\mathrm{d}\rho}\right] + \frac{\partial}{\partial x_i}\left(\frac{\mathrm{d}f}{\mathrm{d}\rho}\rho u_i\right) = 0. \tag{31}$$

This equation is identical to the continuity equation in conservative form (13) under the condition that the quantities $f - \rho\frac{\mathrm{d}f}{\mathrm{d}\rho}$ and $\frac{\mathrm{d}f}{\mathrm{d}\rho}$ are constant in space. Combination of both conditions, results in the requirement that, for mass conservation, f and ρ must be linearly dependent.

3. State equations

In the considered test cases, three different fluid configurations are investigated, each with a different state equation. First, we consider a single fluid ideal gas, with, as equation of state, the ideal-gas law in non-dimensional form:

$$\rho = \frac{p_0}{T}. \tag{32}$$

Next, we consider non-reacting mixing of two fluids A and B, with different density ρ_A and ρ_B. The density of the mixture is a linear function of $\rho\xi$, with the mixture fraction ξ, defined as the mass fraction of fluid A in the mixture. By this definition, $\xi = 1$ in pure A and $\xi = 0$ in pure B.

$$\rho = \rho_B + \left(1 - \frac{\rho_B}{\rho_A}\right)\rho\xi. \tag{33}$$

Finally, in non-premixed reacting flows, we consider an equation of state that consists of two branches, on the lean and rich side of stoichiometry. The lowest density is found at stoichiometry and a simple chemistry model is adopted, resulting in a piecewise linear relationship $\rho = \mathcal{H}_C(\rho\xi)$:

$$\begin{aligned} \rho &= \rho_0 + \frac{\rho_{st} - \rho_0}{\rho_{st}\xi_{st}}\rho\xi \quad \text{for } \xi \leqslant \xi_{st}, \\ \rho &= \rho_0 + \frac{\rho_{st} - \rho_0}{\rho_0 - \rho_{st}\xi_{st}}(\rho_0 - \rho\xi) \quad \text{for } \xi \geqslant \xi_{st}. \end{aligned} \tag{34}$$

This state equation is non-differentiable in the stoichiometric point, and forms therefore a challenge for the algorithms to perform well.

In the remainder, the following dimensional values will be used: $\rho_A = 1\ \mathrm{kg/m^3}, \rho_B = 0.1\ \mathrm{kg/m^3}, \rho_0 = 1.25\ \mathrm{kg/m^3}, \rho_{st} = 0.27\ \mathrm{kg/m^3}, \xi_{st} = 0.1$.

4. Pressure-correction schemes

In the literature, two segregated solution procedures are widespread. The first one [2,5,7,11,14,15,23] is a direct extension of the incompressible constant density pressure-correction algorithm. The continuity equation is used to form a Poisson equation for the pressure-correction. We refer to this algorithm as the continuity-constraint pressure-correction scheme. As mentioned in the introduction, it suffers from instability problems if the density ratio gets high. The continuity-constraint pressure-correction schemes in the cited references all differ somewhat. These differences, however, are related only to the extension of the basic scheme to all-speed applications, the higher-order formulation or the choice of the spatial discretization. For application to the low-Mach number equations treated in this paper, the methodology is unique, as described in Section 4.1.

The second scheme, [1,6,13,15,18,20,21] mostly is called a projection method. The pressure correction equation is obtained from the compatibility constraint on the divergence of the velocity field, as derived in Section 2.1, i.e. Eq. (17), or more generally a compatibility constraint obtained by combination of the continuity equation and a second equation determining density under given thermodynamic pressure, i.e. the energy equation or the mixture fraction equation, as derived in Section 2.2, i.e. Eq. (28). A preliminary value of the velocity field is obtained from the momentum equation. This velocity field, in general, does not satisfy the divergence constraint and the velocity field is projected onto a field which satisfies this

constraint. Strictly, a projection is only possible when the constraint is: divergence of the velocity equal to zero, which applies to constant density flows or flows for ideal gas at constant temperature. The origin of the term comes from constant density flows, and the term mostly is also used for more general flows. We refer here to a method of this type as a compatibility-constraint pressure-correction method. The compatibility-constraint method based on an analytically derived constraining equation for the velocity field assumes differentiability of the equation of state. As will be shown hereafter, the error can be large if non-differentiability occurs. To cure the error with respect to the equation of state, we propose here a new method where the compatibility equation is obtained by combination of the discretized forms of the continuity equation and the energy equation, or the equation replacing the energy equation. We call this new method the discrete compatibility-constraint pressure-correction method. We call the existing class of projection methods the analytical compatibility-constraint pressure-correction methods. Some of the differences between the methods in the cited works are related to the extension to all-speed flows, higher-order accurate formulations or the spatial discretization. For application to low-Mach number flows in this paper, the methods can be classified into three variants, as described in Section 4.2.

Hereafter, we describe the three types of methods. For simplicity, the discrete equations are presented for one-dimensional flows, but extension to two or three dimensions is straightforward. We use the velocity-staggered formulation in order to avoid odd–even decoupling. The staggered formulation is the simplest. Extension to colocated formulation is possible. For a discussion on this aspect, we refer to [16], where an analytical compatibility-constraint pressure-correction method is used. The two dimensional mixing layer examples in this paper are calculated with a colocated method. For simplicity, in the first tests a first order upwind discretization is applied to the convective terms and the time-stepping is first order. The derivation of the schemes is not restricted to first order upwinding and higher order time accuracy can easily be achieved, using a multistage loop. At first, we restrict ourselves to first order formulations, in order to rule out differences between methods that are related to higher order formulations. Extension to higher order is demonstrated with the examples of Sections 5.3 and 7.

4.1. Continuity-constraint pressure-correction

This scheme is a direct extension of the constant-density pressure correction [3,4]. The velocity field must satisfy the continuity equation. First, a predictor step for momentum is taken, with the value of the pressure at the previous time step:

$$\frac{(\rho u)^*_{i+\frac{1}{2}} - (\rho u)^n_{i+\frac{1}{2}}}{\Delta t} = -\frac{(\rho u)^n_R u^n_{i+1} - (\rho u)^n_L u^n_i}{\Delta x} - \frac{p^n_{i+1} - p^n_i}{\Delta x} + Visc^n_{i+\frac{1}{2}}, \tag{35}$$

where the subscripts R and L indicate extrapolated values at the right and left face of the control volume. For first order upwinding, and positive values of the velocity, this means $(\rho u)_R = \rho_{i+\frac{1}{2}} u_{i+\frac{1}{2}}$ and $(\rho u)_L = \rho_{i-\frac{1}{2}} u_{i-\frac{1}{2}}$, with averaged face density values: $\rho_{i+\frac{1}{2}} = (\rho_i + \rho_{i+1})/2$. The node velocities are calculated by averaging: $u_i = \left(u_{i-\frac{1}{2}} + u_{i+\frac{1}{2}}\right)\Big/2$.

The viscous flux is discretized centrally. This means $Visc_{i+\frac{1}{2}} = \frac{1}{Re_\infty}\frac{\tau_{i+1}-\tau_i}{\Delta x}$ and $\tau_i = \mu\frac{u_{i+\frac{1}{2}}-u_{i-\frac{1}{2}}}{\Delta x}$. The final momentum equation to be solved is:

$$\frac{(\rho u)^{n+1}_{i+\frac{1}{2}} - (\rho u)^n_{i+\frac{1}{2}}}{\Delta t} = -\frac{(\rho u)^n_R u^n_{i+1} - (\rho u)^n_L u^n_i}{\Delta x} - \frac{p^{n+1}_{i+1} - p^{n+1}_i}{\Delta x} + Visc^n_{i+\frac{1}{2}}. \tag{36}$$

Subtracting Eq. (36) from Eq. (35), yields:

$$\frac{(\rho u)'_{i+\frac{1}{2}}}{\Delta t} = -\frac{p'_{i+1} - p'_i}{\Delta x}, \tag{37}$$

with $(\rho u)' = (\rho u)^{n+1} - (\rho u)^*$ and $p' = p^{n+1} - p^n$ the momentum and pressure corrections.

The spatial derivatives in the continuity equation (13) are discretized at time level $n+1$:

$$\frac{\rho^{n+1}_i - \rho^n_i}{\Delta t} = -\frac{(\rho u)^{n+1}_{i+\frac{1}{2}} - (\rho u)^{n+1}_{i-\frac{1}{2}}}{\Delta x}. \tag{38}$$

The face mass fluxes at level $n+1$ are defined as the predicted momentum values from (35) plus the corrections given by (37). Substitution of the corrections gives:

$$\frac{\rho^{n+1}_i - \rho^n_i}{\Delta t} = -\frac{(\rho u)^*_{i+\frac{1}{2}} - (\rho u)^*_{i-\frac{1}{2}}}{\Delta x} - \frac{\frac{p'_{i-1}-p'_i}{\Delta x} - \frac{p'_i - p'_{i+1}}{\Delta x}}{\Delta x} = -\frac{(\rho u)^*_{i+\frac{1}{2}} - (\rho u)^*_{i-\frac{1}{2}}}{\Delta x} - \frac{p'_{i-1} - 2p'_i + p'_{i+1}}{\Delta x^2}. \tag{39}$$

The value ρ^{n+1}_i in Eq. (38) follows from the temperature equation:

$$\frac{T^{n+1}_i - T^n_i}{\Delta t} = -u^n_i\frac{T^n_R - T^n_L}{\Delta x} + Cond(T^n) + Press(\rho^n, p_0), \tag{40}$$

with $\rho^{n+1}_i = p^{n+1}_0/T^{n+1}_i$. $Cond(T) = \frac{1}{\rho Re_\infty Pr_\infty}\frac{\partial}{\partial x}\left(\kappa\frac{\partial T}{\partial x}\right)$ and $Press(\rho, p_0) = \frac{\gamma-1}{\gamma\rho}\frac{dp_0}{dt}$. In this formulation, $\frac{dp_0}{dt}$ is either prescribed or follows from a global equation over the entire domain (see e.g. [16]).

In case of reacting flows, the density is calculated from the mixture fraction

$$\frac{(\rho\xi)_i^{n+1}-(\rho\xi)_i^n}{\Delta t}=-\frac{(\rho u)_{i+\frac{1}{2}}^n\xi_R^n-(\rho u)_{i-\frac{1}{2}}^n\xi_L^n}{\Delta x}+Diff(\xi^n), \tag{41}$$

with $\rho_i^{n+1}=\rho((\rho\xi)_i^{n+1})$ and $Diff(\xi)=\frac{1}{Re_\infty Pr_\infty Le_\infty}\frac{\partial}{\partial x}\left(\rho D\frac{\partial\xi}{\partial x}\right)$. As mentioned, this scheme suffers from stability problems when the density variations become high.

4.2. Analytical compatibility-constraint pressure-correction

In this approach, corrections are made on the velocity u instead of the momentum (ρu). A predicted value for the velocity is obtained from (35), with

$$u^*=\frac{(\rho u)^*}{\rho^{n+1}}. \tag{42}$$

The predicted velocity field does not obey the compatibility constraint for the divergence of the velocity field and is therefore corrected. Corrections for the velocity and pressure are defined by $u^{n+1}=u^*+u'$ and $p^{n+1}=p^n+p'$. The corrections are linked by writing (37) as

$$\frac{\rho_{i+\frac{1}{2}}^{n+1}u'_{i+\frac{1}{2}}}{\Delta t}=-\frac{p'_{i+1}-p'_i}{\Delta x}. \tag{43}$$

Substitution in the constraint (17) gives:

$$\frac{u_{i+\frac{1}{2}}^{n+1}-u_{i-\frac{1}{2}}^{n+1}}{\Delta x}=\mathrm{RHS}, \tag{44}$$

with

$$\mathrm{RHS}=\frac{-\frac{p_0^{n+1}-p_0^n}{\Delta t}+\gamma\frac{1}{Re_\infty Pr_\infty}\frac{\partial}{\partial x}\left(\kappa\frac{\partial T^{n+1}}{\partial x}\right)}{\gamma p_0^{n+1}} \tag{45}$$

in case of an ideal gas, or, using (28),

$$\mathrm{RHS}=-\frac{1}{Re_\infty Pr_\infty Le_\infty}\left[\frac{\frac{\mathrm{d}\rho}{\mathrm{d}(\rho\xi)}}{\rho-\rho\xi\frac{\mathrm{d}\rho}{\mathrm{d}(\rho\xi)}}\right]_i^{n+1}\frac{\partial}{\partial x}\left(\rho D\frac{\partial\xi^{n+1}}{\partial x}\right) \tag{46}$$

in case of reacting flows at constant thermodynamic pressure, resulting in a variable coefficient Poisson equation for the pressure:

$$-\frac{\Delta t}{\Delta x^2}\left(\frac{p'_{i+1}-p'_i}{\rho_{i+\frac{1}{2}}^{n+1}}-\frac{p'_i-p'_{i-1}}{\rho_{i-\frac{1}{2}}^{n+1}}\right)=\mathrm{RHS}-\frac{u_{i+\frac{1}{2}}^*-u_{i-\frac{1}{2}}^*}{\Delta x}. \tag{47}$$

Several implementation strategies can be followed when using the analytical compatibility-constraint pressure-correction scheme, with different properties in case of a non-linear equation of state. Indeed, as shown with Eq. (31), the conservation of mixture fraction (or energy) and mass, together with the fulfillment of the equation of state, is only possible with a linear $f(\rho)$-dependency. The first variant [15,21] uses the temperature equation (40) or mixture fraction equation (41) to determine, together with the equation of state, the density at the new time level. This method is robust, but does not guarantee mass conservation in case of a non-linear $f(\rho)$-dependency, since the continuity equation is not used in its conservative form. A second variant [13,18,20] determines the density at the new time level, immediately from the continuity equation

$$\frac{\rho_i^{n+1}-\rho_i^n}{\Delta t}=-\frac{\rho_R^n u_{i+\frac{1}{2}}^n-\rho_L^n u_{i-\frac{1}{2}}^n}{\Delta x}. \tag{48}$$

The scalar variable T^{n+1} or ξ^{n+1} is found by inversion of the state equation. This is not always possible, especially in reacting flows. For single fluid ideal gas flow, this variant is extremely attractive since the compatibility constraint is identical to the energy equation in conservative form. So, all equations are then used in their conservative form. For reacting flows, characterized by a non-linear equation of state, the mixture fraction equation is not satisfied in conservative form. Therefore, for reacting flows, most often a third, conservative variant is preferred [1,6,15]. In the conservative variant, the value of the density at the new time level is calculated from the continuity equation (48). In ideal gas flows, the energy equation (17), only determines the overall pressure at the next time level. For reacting flows, the mixture fraction equation (41) is used to calculate mixture fraction in a conservative way. In both cases, the equation of state is not explicitly used. This equation only enters through the analytically obtained compatibility equation (17) or (28). Because the equation of state is only imposed through a material derivative, the solution can drift away from the equation of state if the equation of state is non-linear. The drift can be controlled by means of a penalty term. For reacting flows, the velocity constraint (44) is altered into [6]:

$$\frac{u^{n+1}_{i+\frac{1}{2}} - u^{n+1}_{i-\frac{1}{2}}}{\Delta x} = \mathrm{RHS} + \frac{\zeta}{\Delta t}\frac{\rho_i^{n+1} - \mathcal{H}_C((\rho\xi)_i^{n+1})}{\rho_i^{n+1}}, \tag{49}$$

with $0 < \zeta < 1$ a damping factor.

In the simulation examples, the last variant will be used.

4.3. Discrete compatibility-constraint pressure-correction

As will be illustrated later, the previous scheme is robust for high density gradients. It has, however, one major drawback, that becomes crucial when the equation of state is non-smooth and/or non-linear: the continuity-equation and the second density-determining equation (temperature or mixture fraction) are analytically combined and, in case of the third variant, the equation of state is not explicitly imposed. Indeed: since the equation of state is only used in differential form, there is no guarantee that the equation of state is satisfied at the next time level. For the ideal gas-formulation (7)–(9), the cited deficiency does not cause problems, due to the simplicity of the equation of state. First, with $p_0 = \rho T$, the conservative form of the temperature equation (15) is exactly the compatibility equation (17). This means that, with the mass conservative variant of the previous scheme, the conservation properties are satisfied. Second, if the temperature in the conduction term of the compatibility equations (44) and (45) is set at the new time level with $T^{n+1} = p_0^{n+1}/\rho^{n+1}$, the equation of state is satisfied at the new time level.

The satisfaction of the equations at the discrete level is not guaranteed with the previous scheme for a less trivial equation of state, such as for reacting flow. It is clear that the compatibility equations (44)–(46) is only well justified when the relationship between ρ and $f = \rho\xi$ is everywhere differentiable. This is typically not the case. Furthermore, the analytically derived constraint only imposes the equation of state in differential form and, consequently, does not guarantee actual satisfaction of the state equation if the equation of state is non-linear. Remark that if variant 1 or 2 were used, as described above, the error then shifts to one of the conservation equations.

The problem of the differentiability and non-linearity of the mixture fraction function $\rho = \mathcal{H}_C(f)$, can be avoided by construction of the compatibility equation at a discrete level. The discrete equations for one-dimensional flow are:

$$\frac{\rho_i^{n+1} - \rho_i^n}{\Delta t} + \frac{\rho_R^n u^n_{i+\frac{1}{2}} - \rho_L^n u^n_{i-\frac{1}{2}}}{\Delta x} = 0, \tag{50}$$

$$\frac{\rho^{n+1}_{i+\frac{1}{2}} u^{n+1}_{i+\frac{1}{2}} - \rho^n_{i+\frac{1}{2}} u^n_{i+\frac{1}{2}}}{\Delta t} + \frac{(\rho u)^n_R u^n_{i+1} - (\rho u)^n_L u^n_i}{\Delta x} = -\frac{p^{n+1}_{i+1} - p^{n+1}_i}{\Delta x} + \frac{1}{Re_\infty}\frac{\partial \tau}{\partial x}, \tag{51}$$

$$\frac{f_i^{n+1} - f_i^n}{\Delta t} + \frac{f_R^n u^n_{i+\frac{1}{2}} - f_L^n u^n_{i-\frac{1}{2}}}{\Delta x} = \frac{1}{Re_\infty Pr_\infty Le_\infty}\frac{\partial}{\partial x}\left(\rho D \frac{\partial \xi}{\partial x}\right). \tag{52}$$

We require that $\rho = \mathcal{H}_C(f)$ at every time level. For time level $n+1$, this means:

$$\rho_i^n - \Delta t \frac{\rho_R^n u^n_{i+\frac{1}{2}} - \rho_L^n u^n_{i-\frac{1}{2}}}{\Delta x} = \mathcal{H}_C\left(f_i^n - \Delta t \frac{f_R^n u^n_{i+\frac{1}{2}} - f_L^n u^n_{i-\frac{1}{2}}}{\Delta x} + \Delta t \frac{1}{Re_\infty Pr_\infty Le_\infty}\frac{\partial}{\partial x}\left(\rho D \frac{\partial \xi}{\partial x}\right)\right). \tag{53}$$

The compatibility equation (53) has to be satisfied at every time level, so also at time level $n+2$, which provides a constraint for the unknown velocity u^{n+1}. Inserting $u^{n+1} = u^* + u'$ then yields

$$\rho_i^* + \rho_i' = \mathcal{H}_C(f_i^* + f_i'), \tag{54}$$

with

$$\rho_i^* = \rho_i^{n+1} - \Delta t \frac{\rho_R^{n+1} u^*_{i+\frac{1}{2}} - \rho_L^{n+1} u^*_{i-\frac{1}{2}}}{\Delta x}, \tag{55}$$

$$f_i^* = f_i^{n+1} - \Delta t \frac{f_R^{n+1} u^*_{i+\frac{1}{2}} - f_L^{n+1} u^*_{i-\frac{1}{2}}}{\Delta x} + \frac{\Delta t}{Re_\infty Pr_\infty Le_\infty}\frac{\partial}{\partial x}\left(\rho D \frac{\partial \xi}{\partial x}\right), \tag{56}$$

$$\rho_i' = -\Delta t \frac{\rho_R^{n+1} u'_{i+\frac{1}{2}} - \rho_L^{n+1} u'_{i-\frac{1}{2}}}{\Delta x}, \tag{57}$$

$$f_i' = -\Delta t \frac{f_R^{n+1} u'_{i+\frac{1}{2}} - f_L^{n+1} u'_{i-\frac{1}{2}}}{\Delta x}. \tag{58}$$

Remark that we obtain a non-linear equation in velocity (or pressure), so that an iteration procedure is necessary. Therefore, (54) can be linearised around f^*, resulting in

$$\rho_i^* + \rho_i' = \mathcal{H}_C(f_i^*) + \frac{\mathrm{d}\mathcal{H}_C}{\mathrm{d}f}(f_i^*) f_i'. \tag{59}$$

Eq. (59) can be written in system notation, with matrices A and B, pressure-correction vector $\underline{p'}$:

Table 1
Summary of the algorithm properties for variable density flows. In case of the continuity-constraint pressure-correction, mass conservation is only guaranteed in open domains, hence the notation between brackets.

	Continuity-constraint	Analytical compatibility-constraint	Discrete compatibility-constraint
Stable results		×	×
Mass conservation	(×)	×	×
Exact fulfillment of equation of state	×		×
Constant coefficient Poisson equation	×		

$$\left(A - \frac{\mathrm{d}\mathcal{H}_C}{\mathrm{d}f}(\underline{f}^*)B\right)\underline{p'} = \mathrm{RHS}, \tag{60}$$

with $RHS = \mathcal{H}_C(\underline{f}^*) - \underline{\rho}^*$. All vectors have the dimension of the number of grid nodes. The system is solvable at low cost if the matrices A and B do not change during iteration. Unfortunately, this is not true, since the matrices are composed of extrapolated values of density and fuel mass, which depend on the sign of the unknown velocity u^{n+1}. The same holds for the RHS, whose value also depends on the sign of u^{n+1}. Since this influence is only secondary, a minor assumption can be introduced at this level, still preserving the consistency of the algorithm: if the extrapolated values of ρ and f are calculated, based on the sign of u^*, instead of u^{n+1}, matrices A and B and vector RHS only need one calculation per time step, saving computing time.

For an internal node, Eq. (60) yields, by combination of (43) and (54):

$$\frac{(\Delta t)^2}{(\Delta x)^2}\left\{\left[\rho_R^{n+1} - \frac{\mathrm{d}\mathcal{H}_C}{\mathrm{d}f}(f_i^*)f_R^{n+1}\right]\frac{p'_{i+1} - p'_i}{\rho_{i+\frac{1}{2}}^{n+1}} - \left[\rho_L^{n+1} - \frac{\mathrm{d}\mathcal{H}_C}{\mathrm{d}f}(f_i^*)f_L^{n+1}\right]\frac{p'_i - p'_{i-1}}{\rho_{i-\frac{1}{2}}^{n+1}}\right\} = \mathcal{H}_C(f_i^*) - \rho_i^*. \tag{61}$$

4.4. Summary

Comparison of the properties of the different pressure-correction schemes, yields the result shown in Table 1. The discrete compatibility constraint pressure-correction scheme (Section 4.3) yields stable results for variable density flows and provides a consistent solution, which is the most vital property missing in the continuity-constraint pressure-correction (Section 4.1). Furthermore, all conservation properties are fulfilled, together with the equation of state. The latter is only approximately fulfilled for the analytical compatibility-constraint pressure-correction scheme (Section 4.2). The only drawback of the discrete compatibility-constraint pressure-correction scheme is that the resulting pressure equation has variable coefficients that require several evaluations every time step. The extra cost, however, is marginal compared to the benefits associated with this algorithm: the higher robustness and the greater accuracy in terms of state prediction.

5. One-dimensional test cases

The properties of the pressure-correction algorithms are now demonstrated on a few well-chosen and simple examples. In this section, we restrict ourselves to one-dimensional tests. Although 1D configurations are insufficient to qualify/disqualify numerical schemes, many valuable insights are gained by these idealized flow configurations. They provide an answer to the question why common pressure-correction algorithms fail to give stable results. We consider a successful simulation in 1D as a necessary condition for the eventual algorithm to yield stable and consistent solutions in any general multi-dimensional variable-density problem (where certain shortcomings may be masked by physical or numerical dissipation and diffusion).

Two different kinds of tests are performed:

- purely convective transport of a sharp (density) gradient in a channel;
- purely diffusive transport of the same gradient.

A combination of these two tests, collects all possibilities in a 1D flow (except for source terms and boundary conditions). The origin of the gradient, depends on the fluid properties. We consider the three fluid configurations of Section 3 and apply the three schemes of Section 4. Thus $2 \times 3 \times 3 = 18$ simulations are performed.

The 1D test cases use a staggered grid topology to avoid possible odd–even decoupling. The transient calculations are performed using a time step of 0.9 times the maximum allowable time step for stability, according to the CFL-criterion. As such, the algorithms are tested, close to the stability limits. For each test, results after 1 and 10 time steps are displayed to illustrate the evolution in time of the different algorithms.

5.1. Pure convection

A step in the scalar variable ϕ (temperature or mixture fraction) is convected in a straight channel. All diffusive terms (conduction and species diffusion) are set to zero. The initial step is defined in space as the piecewise constant function

$$\phi_i = \begin{cases} \phi_1 & \text{for } i \in [1, i_1[, \\ \phi_2 & \text{for } i \in [i_1, i_2], \\ \phi_1 & \text{for } i \in]i_2, N_x]. \end{cases} \tag{62}$$

In this case, an analytical solution exists: the velocity in every section of the channel should remain equal to the imposed inlet velocity and the scalar field is shifted in space, over a distance $u \cdot t$, with $u = 1$ m/s the inlet velocity and t the simulated time. In the problem considered, $N_x = 50$ grid points were used and the step in the scalar field is situated in the grid node interval [10,30]. The grid spacing is set to 1 m, so that the time step is calculated as:

$$\Delta t = 0.9/u_{max}. \tag{63}$$

5.1.1. Single fluid flow: ideal gas

The initial velocity, temperature and density fields are depicted in Fig. 1 (left). A temperature step with a step factor of 10 is used, resulting in a density field, having the same initial ratio.

5.1.1.1. Continuity-constraint pressure-correction. Fig. 2 (top) shows that the continuity-constraint pressure-correction scheme gives inaccurate predictions for the velocity field (dashed line), even in regions far away from the density jump ($x >> 30$). This observation follows from the corrector step (38), imposing mass conservation. Since the density field at the new time level follows from the non-conservative discretization (40), mass is conserved through adjustment of the outlet velocity. As a consequence, errors near sharp gradients do not only have a local impact, but also have a major influence in the entire domain.

The algorithm is also inconsistent, since grid refinement does not remove the problem. The simulation also does not remain stable at later times.

Since the CFL-number is kept constant during the time stepping, with a large maximum value for the velocity in the domain, the actual time evolved is small, which explains why the first density gradient is still around node 10, after 10 time steps.

5.1.1.2. Analytical compatibility-constraint pressure-correction. With variant 3 of Section 4.2, the velocity field does not differ from the exact solution and remains constant in time (Fig. 2, bottom). This is not surprising, since the compatibility constraint for non-diffusive flows simplifies into $\nabla \cdot \mathbf{u} = 0$, for a 1D problem resulting in a constant velocity field. The density field does show some deviation from the exact solution, but this observation is an artefact of the first order upwind scheme for the convective fluxes.

Note that, in contrast to the previous simulation, the time step does not vary (as the velocity remains constant), so that the first step in temperature is already convected further downstream.

5.1.1.3. Discrete compatibility-constraint pressure-correction. In the case of an ideal gas, the constraining equation for the compatibility-constraint pressure-correction is identical with the analytical and the discrete derivation, so that the same results as Fig. 2 (bottom) are obtained.

5.1.2. Two fluid flow: inert mixing

The initial velocity, fuel elements density and density fields are depicted in Fig. 1 (center). Initially, fluid B is surrounded by fluid A, with $\rho_B : \rho_A = 1 : 10$.

5.1.2.1. Continuity-constraint pressure-correction. Again, Section 4.1 predicts an erroneous result (Fig. 3, top). However, since fuel elements density is predicted in a conservative way (41) and the density is a linear function of fuel elements density

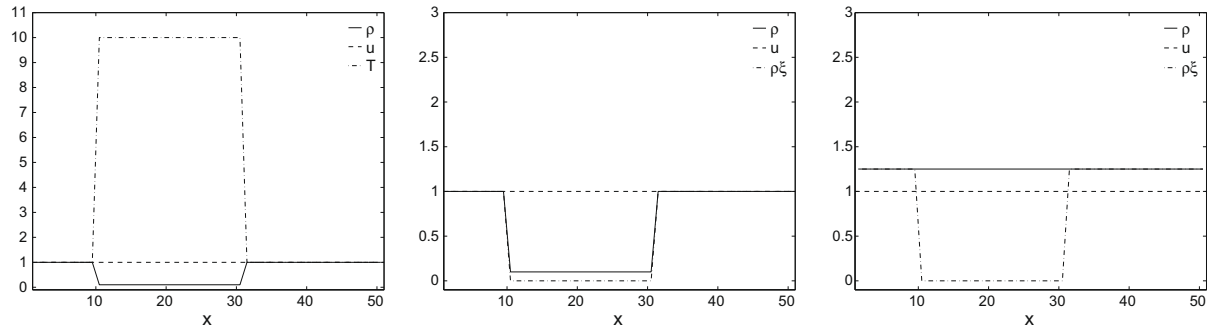

Fig. 1. Purely convective transport of a temperature step in an ideal gas (left), of two inert mixing fluids with different densities (center) and of two reacting fluids (right) in a straight channel: initial condition.

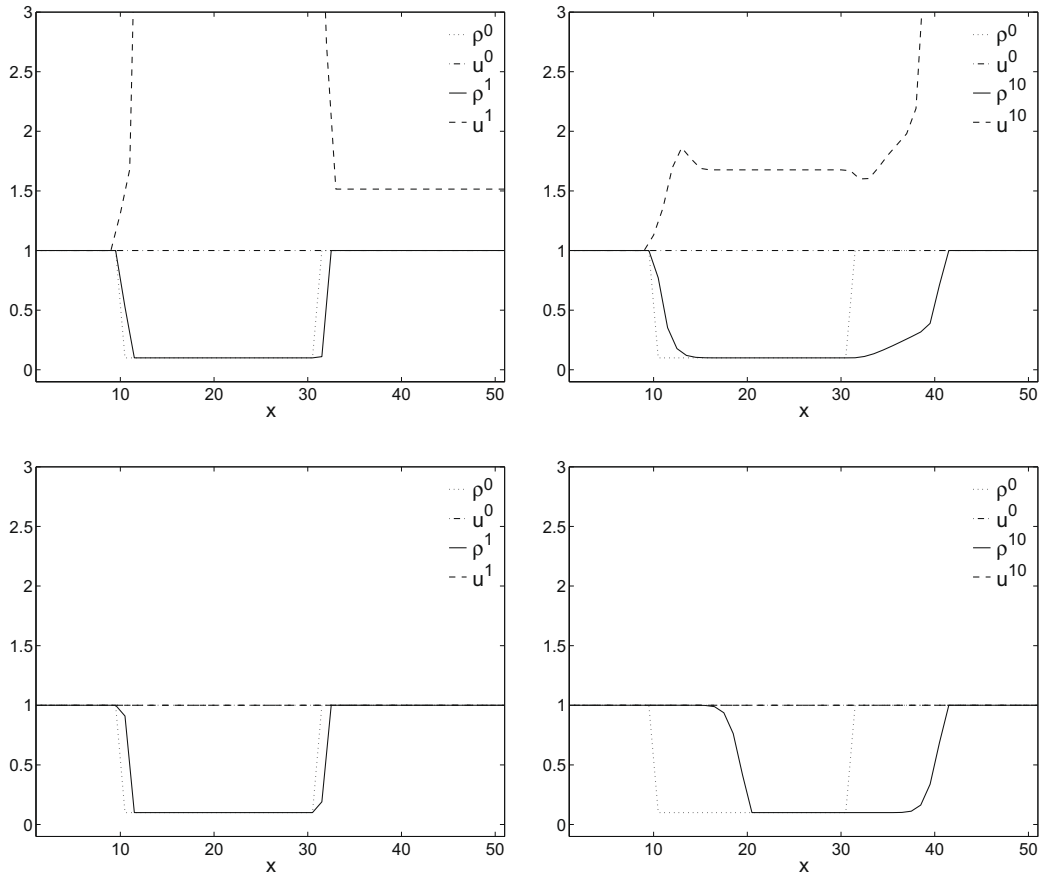

Fig. 2. Density and velocity fields, obtained with the continuity-constraint (top) and the compatibility constraint (bottom) pressure-correction algorithm after 1 (left) and 10 (right) time steps for pure convection of a temperature step in an ideal gas. Use of the continuity constraint results in inaccurate predictions for the velocity field, even in the region far from the density jump ($x \gg 30$). A consistent prediction for the velocity field is obtained, using the compatibility constraint, with identical results for the analytical and discrete version of the algorithm.

(33), the predictor step is mass conserving. As a consequence, possible errors induced by the requirement of mass conservation by the corrector step (38), remain localized near sharp gradients.

Note that physically impossible values are obtained for the density ($\rho > 1$ kg/m^3). This is a result of the fuel elements density prediction, where in this case only the mixture fraction is upwinded (41). The mass flux ρu is not constant in space and leads to local flow compression or expansion.

The equation of state is automatically fulfilled at every time step, because the new density field is determined from the mixture fraction prediction, precisely using the equation of state.

The solution becomes unstable at later times.

5.1.2.2. Analytical compatibility-constraint pressure-correction. Because of the same reason as the ideal gas case, the exact velocity field is also obtained in case of inert mixing (Fig. 3, bottom).

The fulfillment of the state equation is verified by plotting density against fuel elements density. Fig. 4 shows that at every time step, density and fuel elements density are predicted according to the equation of state. This result is no surprise, since, also in case of inert mixing, the constraining equation is the same whether the analytical or the discrete compatibility is expressed. Results obtained with the analytical scheme will therefore not differ from the ones obtained with the discrete scheme, which is especially designed to obtain results that exactly obey the equation of state.

5.1.2.3. Discrete compatibility-constraint pressure-correction. As discussed above, Fig. 3 (bottom) and Fig. 4 also apply for this algorithm.

5.1.3. Two-fluid flow: non-premixed combustion

The initial velocity, fuel elements density and density fields are depicted in Fig. 1 (right). Initially, the oxidizer is surrounded by fuel with the same density. The properties of fuel, oxidizer and mixture are gained from Eq. (34).

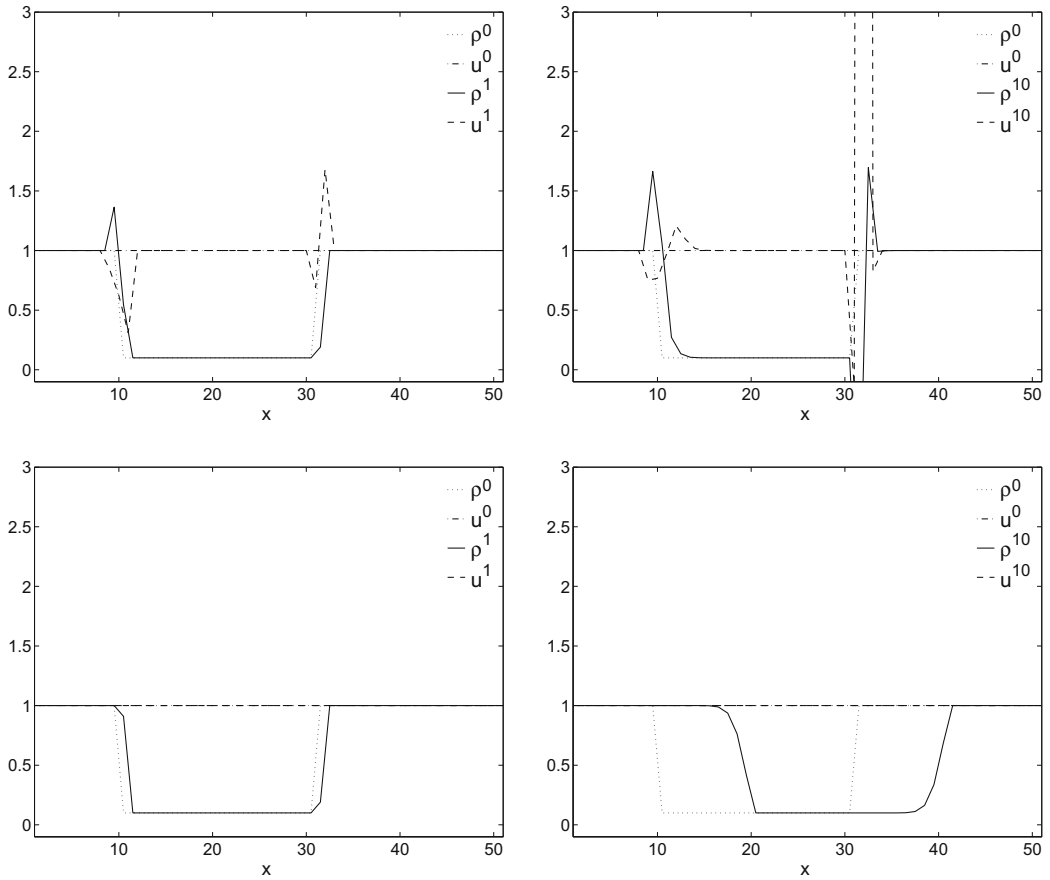

Fig. 3. Density and velocity fields, obtained with the continuity-constraint (top) and the compatibility constraint (bottom) pressure-correction algorithm after 1 (left) and 10 (right) time steps for pure convection of inert mixing fluids. Use of the continuity constraint results in inaccurate predictions for the velocity field, close to density jumps. A consistent prediction for the velocity field is obtained, using the compatibility constraint, with identical results for the analytical and discrete version of the algorithm.

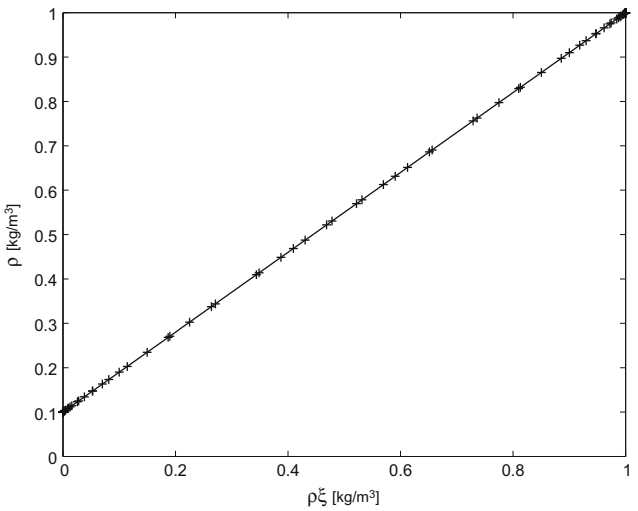

Fig. 4. Scatter plot of the obtained density and fuel elements density predictions during 10 time steps in the simulation of pure convection of inert mixing fluids with the compatibility-constraint pressure-correction algorithm. Density and fuel elements density are predicted according to the equation of state (full line).

5.1.3.1. Continuity-constraint pressure-correction. This time, the first time step is relatively well predicted (Fig. 5, top left), due to the constant initial density and velocity in the entire domain. At the interfaces between fuel and oxidizer, the density deviates from its constant value, due to numerical diffusion in the mixture fraction prediction. As a consequence, numerical mixing occurs between fuel and oxidizer, yielding a lower density due to reaction. Because mass has to be conserved in the corrector step (38), a local lower density requires flow acceleration towards the outlet, as can be seen in the figure (dashed line).

In the next time steps (Fig. 5, top right), the velocity and density fields are no longer constant, and the solution gets worse. Velocity fields that differ several orders of magnitude from the exact solution can be noticed (dashed line) as well as unphysical values (higher than the initial value) of the density field (solid line).

The solution becomes unstable at later times.

5.1.3.2. Analytical compatibility-constraint pressure-correction. Based on the simulation results of Fig. 5 (bottom), Section 4.2 seems ideal, because the density and velocity fields exactly correspond to the analytical solution. However, the scatter plot of the obtained states, Fig. 6 (top left) reveals big discrepancies between the predicted density and fuel elements density fields and the equation of state. Indeed, due to numerical diffusion, the step in mixture fraction is smoothed during convection, so that intermediate states are obtained. However, the analytical expression for the constraint does not guarantee that densities match the equation of state. The discrepancies can be controlled by incorporating a penalty term in the constraining equation. Results for this test case, using a damping factor $\zeta = 0.5$, Eq. (49), are shown in Fig. 7 (top) and Fig. 6 (top right). The scatter plot, reveals predicted states that are indeed closer to the equation of state. Density and velocity fields are no longer exact, but suffer from numerical diffusion due to upwinding in the convective fluxes, as already explained.

5.1.3.3. Discrete compatibility-constraint pressure-correction. In case of non-premixed combustion, the discrete formulation of the constraint differs from the analytical one, leading to different results (Fig. 7, bottom). A reaction zone, characterised by a

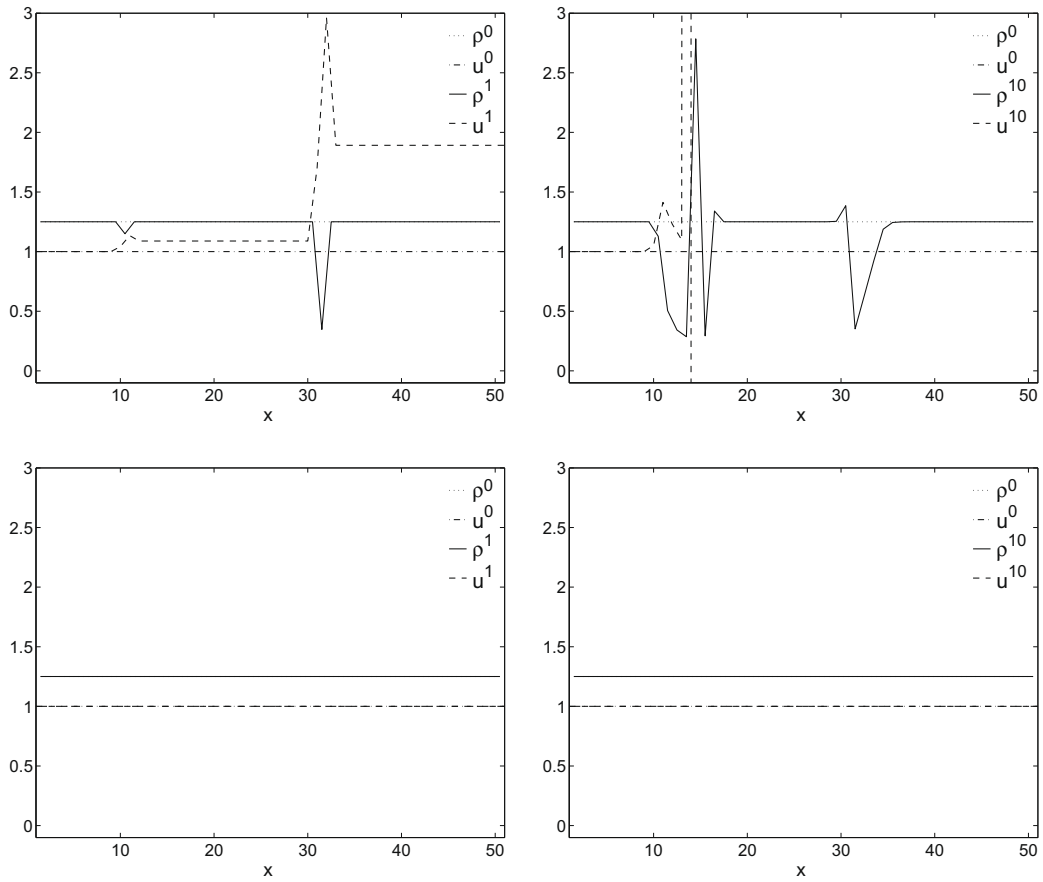

Fig. 5. Density and velocity fields, obtained with the continuity-constraint (top) and the analytical compatibility constraint (bottom) pressure-correction algorithm after 1 (left) and 10 (right) time steps for pure convection of reacting fluids. Use of the continuity constraint yields a velocity field that differs several orders of magnitude from the exact solution. Solutions for the velocity field do not differ from the exact solution, using the analytical compatibility constraint algorithm.

lower density, can be noticed at the interfaces between fuel and oxidizer and, consequently, the flow accelerates towards the outlet. This is caused by numerical diffusion: due to the first order upwinding of the convective terms, the initial step in the mixture fraction field is smoothed, resulting in intermediate mixture fraction values, whose corresponding density is lower, according to the equation of state.

In contrast to the continuity-constraint pressure-correction scheme, the compatibility-constraint pressure correction yields stable results, that are physically possible. In the discrete version, the predicted states correspond exactly to the equation of state (Fig. 6, bottom).

To obtain this exact correspondence, a price must be paid. The constraining equation (54) is now a non-linear equation in u', so that several iterations are needed to obtain the solution. Performing a linearisation (59), for this problem only two iterations of Newton's method were needed to solve the non-linear system. In more general flows, more iterations will be needed. Still, if Newton's method is applied in a smart way, as discussed in Section 4.3, only a minimal additional effort is spent, since the elliptic pressure equation already requires an iterative solution procedure for realistic problems.

5.2. One-dimensional pure diffusion/conduction

Initially, the velocity is zero everywhere in the domain but diffusive transport occurs through conduction or species diffusion. The values for the diffusive constants are $\lambda = 1$ W/(m K) in case of a single fluid ideal gas and $\rho D = 1$ Pa s in case of two fluid flow. It should be noted that non-zero velocities occur during the simulation, giving rise to a convective part. Since this is only a secondary effect, the term 'pure diffusion' is used to describe this series of test cases.

In the resulting test case, diffusion takes place, at a step in the scalar variable ϕ (temperature or mixture fraction) in a straight channel. The initial step is defined in space as the piecewise constant function

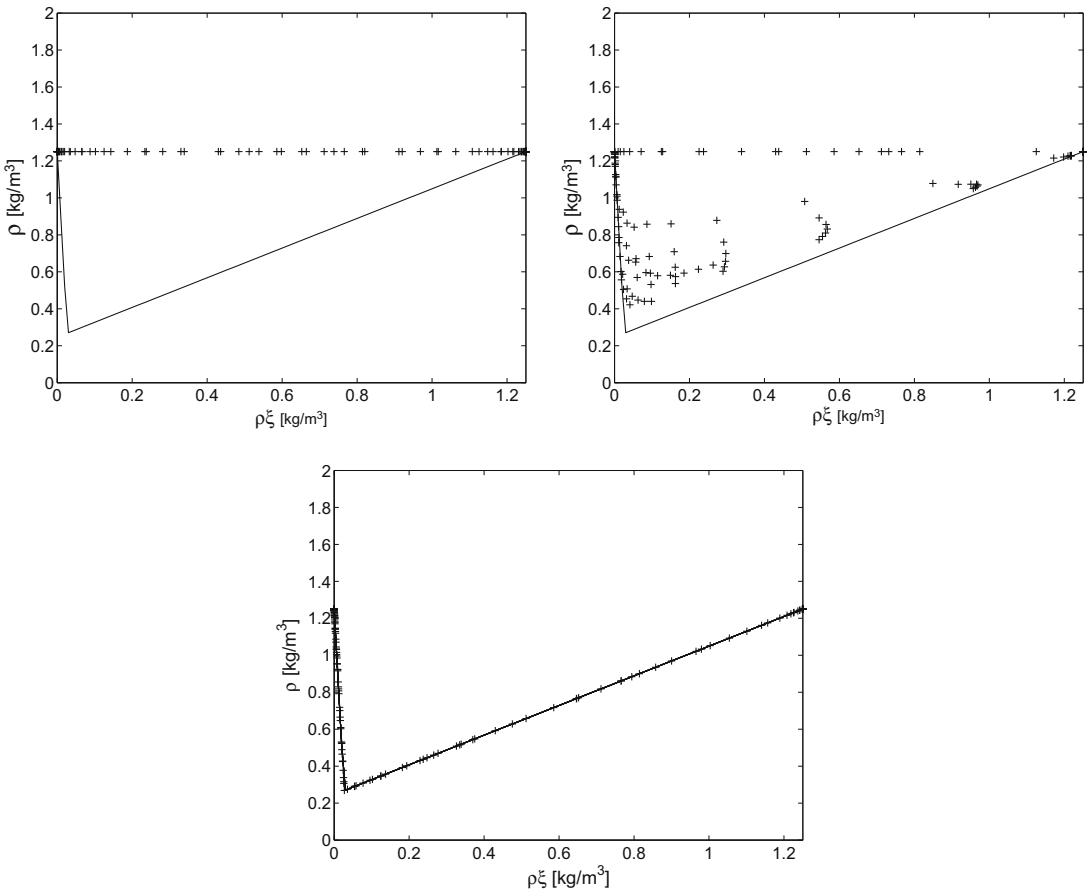

Fig. 6. Scatter plot of the obtained density and fuel elements density predictions during 10 time steps in the simulation of pure convection of reacting fluids with the analytical compatibility-constraint pressure-correction algorithm without penalty term (top left), using a damping factor $\zeta = 0.5$ in the penalty term (top right) and with the discrete compatibility-constraint pressure-correction algorithm (bottom). The drift from the equation of state (full line) is controlled using a penalty term in the analytical compatibility constraint, but exact correspondence can only be obtained using the discrete compatibility constraint.

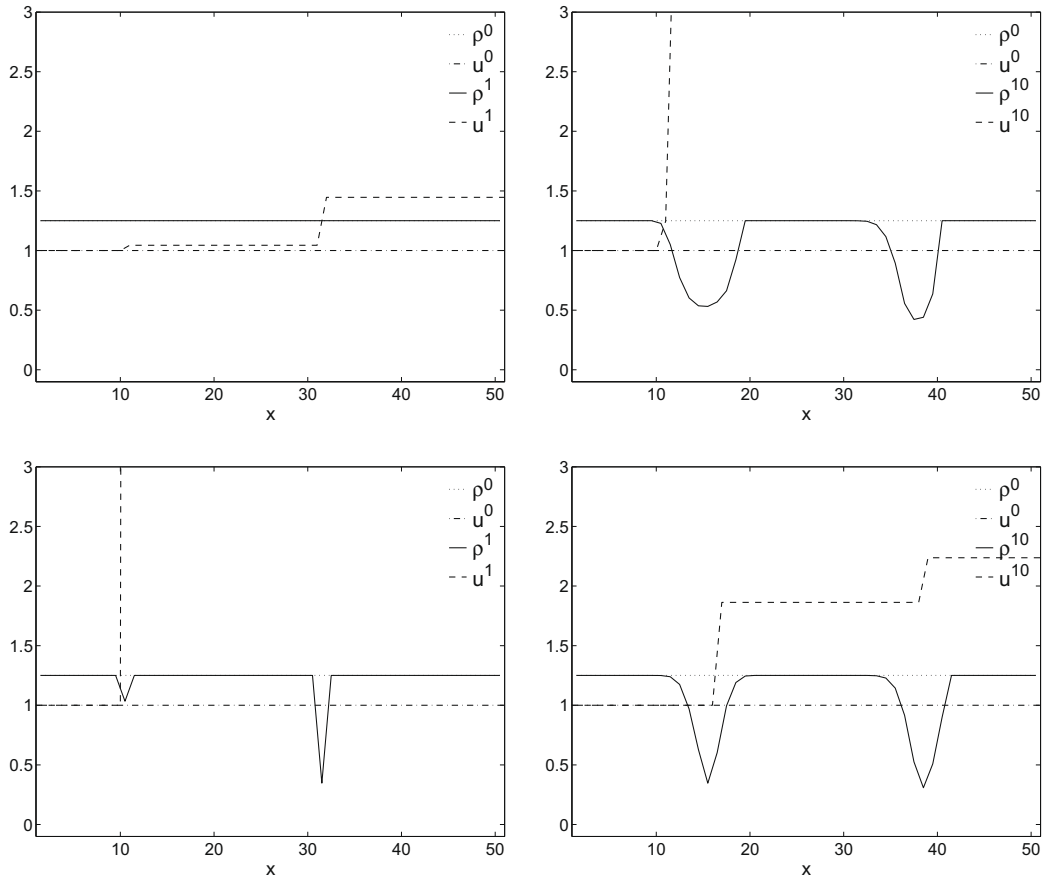

Fig. 7. Density and velocity fields, obtained with the analytical compatibility-constraint with damping factor $\zeta = 0.5$ (top) and the discrete compatibility constraint (bottom) pressure-correction algorithm after 1 (left) and 10 (right) time steps for pure convection of reacting fluids. The drift from the equation of state is controlled using a penalty term in the analytical compatibility constraint, but exact correspondence can only be obtained using the discrete compatibility constraint, yielding a solution that only differs from the exact solution because of upwinding. Values for the velocity, exceeding the axis: $u = 350$ m/s (top right), $u = 56$ m/s (bottom left).

$$\phi_i = \begin{cases} \phi_1 & \text{for } i \in [1, i_1], \\ \phi_2 & \text{for } i \in]i_1, N_x]. \end{cases} \tag{64}$$

In this case, no analytical solution exists. In the problem considered, $N_x = 50$ grid points were used and the step in the scalar field is situated at grid node 20. The grid spacing is set to 1 m. At the left boundary a velocity of 0 is imposed, whereas the velocity is let free at the right boundary.

It will become clear in this section that results for pure diffusion show the same tendencies as in the pure convection case, but a diffusive flow appears less sensitive than a purely convective flow.

5.2.1. Single fluid flow: ideal gas

The initial velocity, temperature and density fields are depicted in Fig. 8 (left). A temperature step with a step factor of 10 is used, resulting in a density field, having the same initial ratio.

5.2.1.1. Continuity-constraint pressure-correction. For this test case, the continuity-constraint pressure-correction algorithm remains stable (Fig. 9, top). However, due to the non-mass-conserving prediction of temperature (and density), inaccurate velocity fields are predicted, even in regions far away from the diffusion layer.

The solution remains also stable at later times.

5.2.1.2. Analytical compatibility-constraint pressure-correction. This algorithm shows stable and consistent predictions for conductive flows (Fig. 9 bottom). A positive velocity field near the diffusion zone ensures mass transport from the high-density region ($x < 20$) to the low-density region ($x > 20$). At the outlet, the velocity remains zero, as it should: since there is no reaction, the flow should not display overall acceleration.

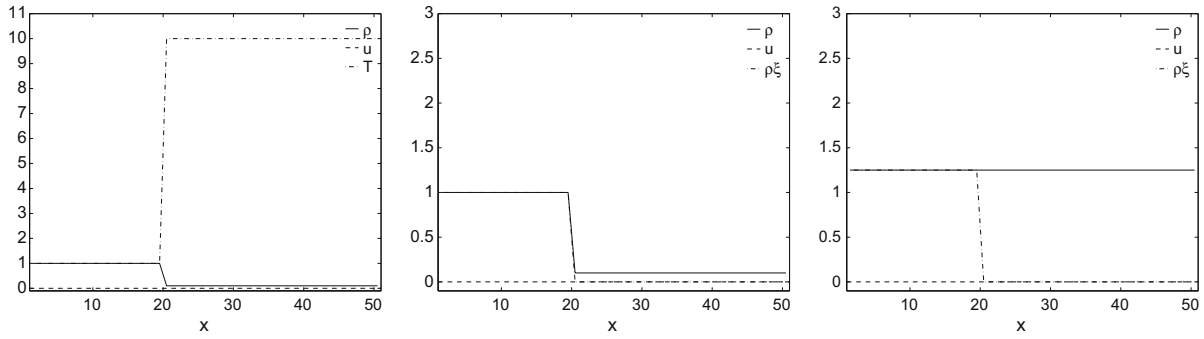

Fig. 8. Purely diffusive transport of a temperature step in an ideal gas (left), of two inert mixing fluids with different densities (center) and of two reacting fluids (right) in a straight channel: initial condition.

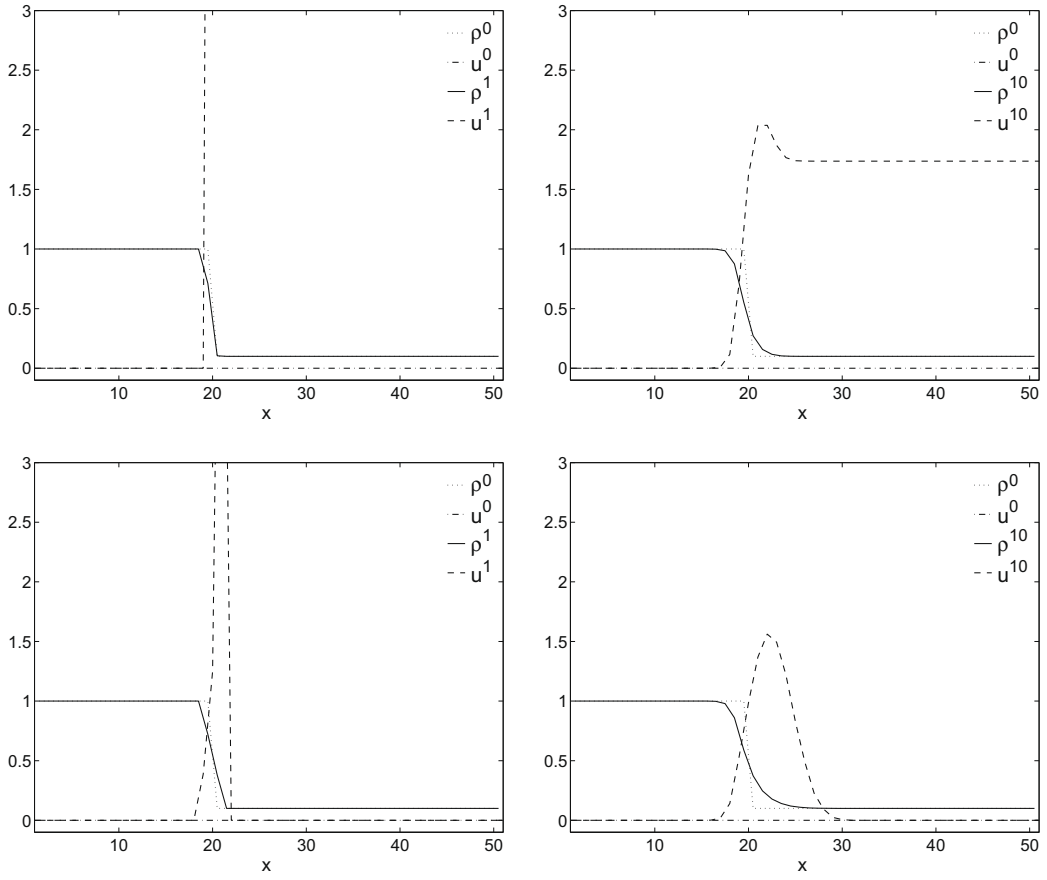

Fig. 9. Density and velocity fields, obtained with the continuity-constraint (top) and the compatibility constraint (bottom) pressure-correction algorithm after 1 (left) and 10 (right) time steps for pure conduction of a temperature step in an ideal gas. Use of the continuity constraint results in inaccurate predictions for the velocity field, even in the region far from the density jump ($x \gg 20$). A consistent prediction for the velocity field is obtained, using the compatibility constraint, with identical results for the analytical and discrete version of the algorithm. Values for the velocity, exceeding the axis: $u = 63$ m/s (top left), $u = 7.4$ m/s (bottom left).

5.2.1.3. Discrete compatibility-constraint pressure-correction. The results are identical to the analytical compatibility-constraint pressure-correction scheme (Fig. 9, bottom).

5.2.2. Two fluid flow: inert mixing

The initial velocity, fuel elements density and density fields are depicted in Fig. 8 (center). Initially, two fluids *A* and *B* are placed next to each other. The two fluids are characterised by densities, that differ with a ratio of 1:10.

5.2.2.1. Continuity-constraint pressure-correction. The flow field is qualitatively well predicted (Fig. 10, top). Especially the zero velocity at the right boundary is noticeable, originating from a mass conserving predictor step.

Also at later times, the result is stable.

5.2.2.2. Analytical compatibility-constraint pressure-correction. A good prediction of density and velocity fields is obtained (Fig. 10, bottom), with predicted states that match the equation of state exactly (Fig. 11).

5.2.2.3. Discrete compatibility-constraint pressure-correction. Results are identical to the analytical compatibility-constraint pressure-correction scheme, Fig. 10 (bottom) and Fig. 11.

5.2.3. Two-fluid flow: non-premixed combustion

The initial velocity, fuel elements density and density fields are depicted in Fig. 8 (right). Initially, fuel and oxidizer, having the same density are placed next to each other. The properties of fuel and oxidizer and its mixtures are gained from Eq. (34).

5.2.3.1. Continuity-constraint pressure-correction. Fig. 12 (top) shows the results for the continuity-constraint pressure-correction. Wiggles appear in the solution for the velocity. Already after 10 time steps, the velocity field deviates several orders of magnitude from the exact solution and the solution is unstable.

5.2.3.2. Analytical compatibility-constraint pressure-correction. Using the analytical compatibility-constraint pressure-correction method, a stable simulation can be performed, yielding at first sight (Fig. 12, bottom) acceptably accurate results. Remarkable is the bump in the density field after 10 time steps. The scatter plot (Fig. 13, top left) reveals that this is due to deviations of the predicted density and fuel elements density fields from the equation of state.

Inclusion of a penalty term in the corrector step, with $\zeta = 0.5$, Eq. (49), alleviates the difference between the predicted state and the state equation (Fig. 13, top right) and removes the bump in the density field (Fig. 14, top right).

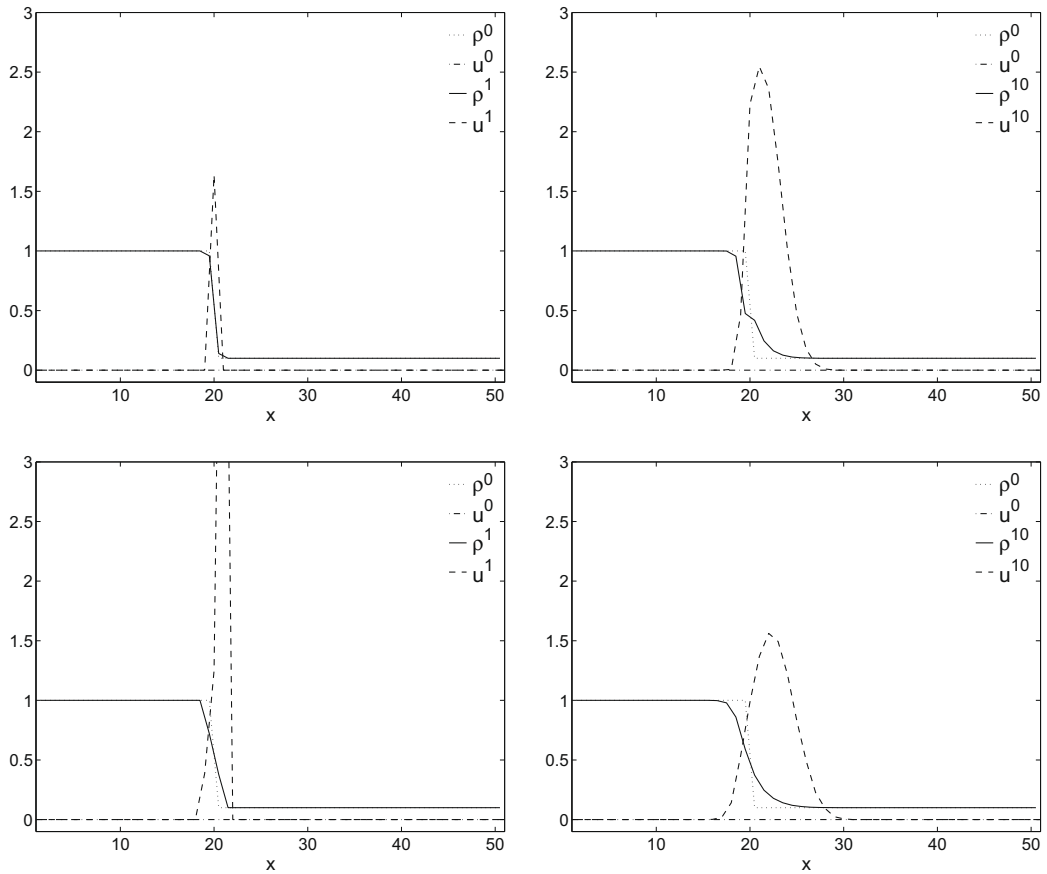

Fig. 10. Density and velocity fields, obtained with the continuity-constraint (top) and the compatibility constraint (bottom) pressure-correction algorithm after 1 (left) and 10 (right) time steps for pure diffusion of inert mixing fluids. Use of the continuity constraint results in inaccurate predictions for the velocity field, close to density jumps. A consistent prediction for the velocity field is obtained, using the compatibility constraint, with identical results for the analytical and discrete version of the algorithm. Value for the velocity, exceeding the axis: $u = 7.4$ m/s (bottom left).

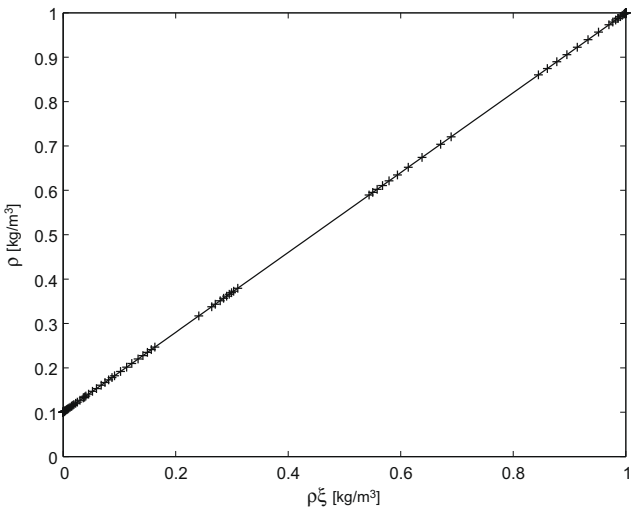

Fig. 11. Scatter plot of the obtained density and fuel elements density predictions during 10 time steps in the simulation of pure diffusion of inert mixing fluids with the compatibility-constraint pressure-correction algorithm. Density and fuel elements density are predicted according to the equation of state (full line).

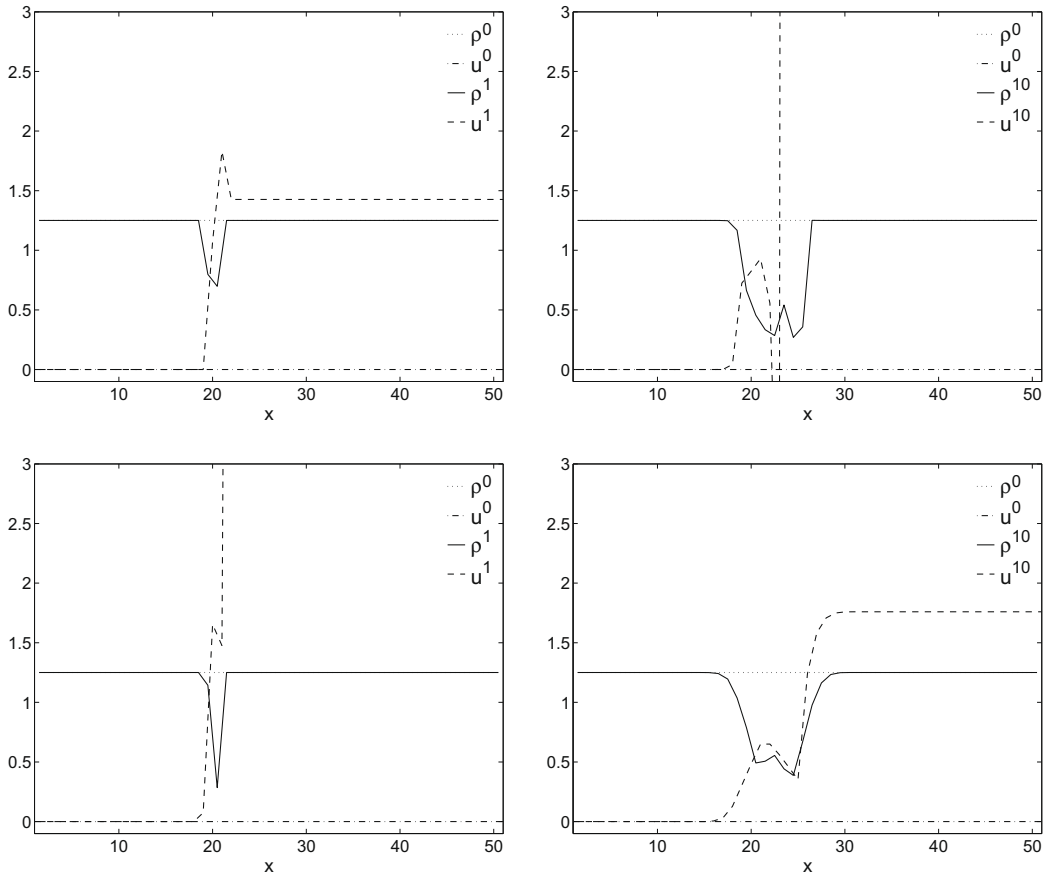

Fig. 12. Density and velocity fields, obtained with the continuity-constraint (top) and the analytical compatibility constraint (bottom) pressure-correction algorithm after 1 (left) and 10 (right) time steps for pure diffusion of reacting fluids. Use of the continuity constraint yields a velocity field that differs several orders of magnitude from the exact solution. Inaccurate results are obtained due to the drift from the equation of state, using the analytical compatibility constraint algorithm. Value for the velocity, exceeding the axis: $u = 15.2\text{m/s}$ (bottom left).

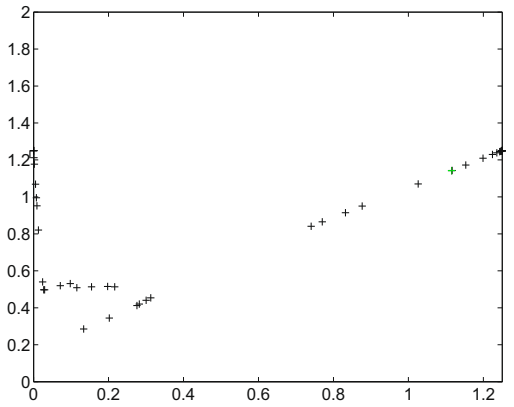

5.2.3.3. Discrete compatibility-constraint pressure-correction. The discrete compatibility-constraint pressure-correction algorithm leads to good results for all state variables (Fig. 14, bottom), with exact fulfillment of the equation of state (Fig. 13, bottom). To achieve this exact correspondence, again mostly one, at maximum two iterations of Newton's method were needed during the inversion of the non-linear pressure Poisson-like Eq. (54).

5.3. Extension to higher order and grid refinement

With the previous examples, we showed that the continuity-constraint pressure-correction algorithm suffers from severe stability problems. Also, particularly in case of pure convection of combusting gases, the analytical compatibility-constraint pressure-correction method without penalty term cannot predict states that are in agreement with the equation of state and the errors with respect hereto are large. The latter behavior will not change when higher order discretizations or finer grids are used. It will become clear from the more-dimensional test cases (Section 7) that these errors can have a serious impact on the overall solution and can even lead to false solutions. Again, in the more-dimensional tests, we will show that the inclusion of a penalty term leads to better solution. The exact fulfillment of the equation of state (discrete compatibility) is even better. Hence, in this section, we investigate the behavior for higher order discretization and grid refinement of the two remaining schemes, i.e. the analytical compatibility-constraint pressure-correction with penalty term and the discrete compatibility-constraint pressure-correction, for the non-linear equation of state (non-premixed combustion).

For reasons of monotonicity, higher order accuracy in space is achieved, using a TVD-scheme. The limiter function is chosen as Roe's superbee flux-limiter. Higher order accuracy in time is adopted, using a low-storage Runge–Kutta scheme with four stages, with an evaluation of the pressure at each stage. The tests were performed using a constant time step of $\Delta t = 0.005$ s. The time step corresponds to a CFL-number at the inlet of $CFL = 0.005$. During the initial time steps, high values for the velocity are obtained because of numerical diffusion, requiring such a small time step. Afterwards, the values for the velocity decrease, yielding a simulation very well below the stability limit.

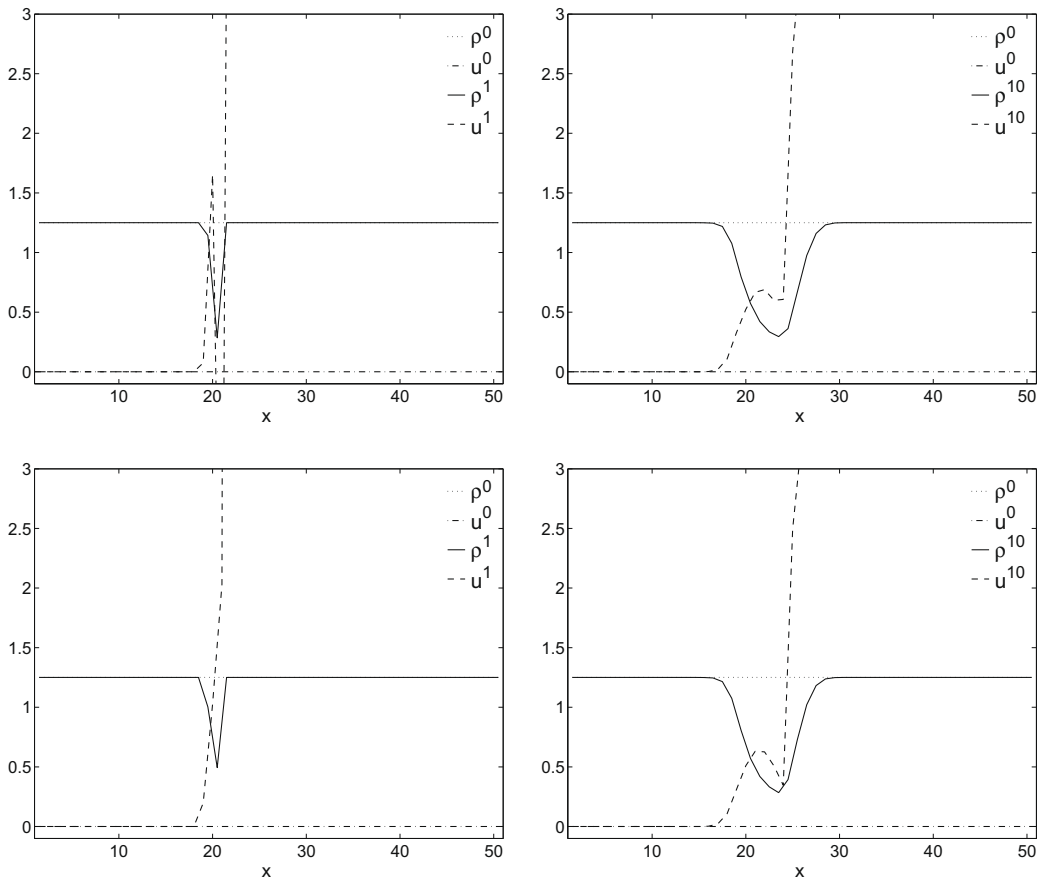

Fig. 14. Density and velocity fields, obtained with the analytical compatibility-constraint with damping factor $\zeta = 0.5$ (top) and the discrete compatibility constraint (bottom) pressure-correction algorithm after 1 (left) and 10 (right) time steps for pure diffusion of reacting fluids. The drift from the equation of state is controlled using a penalty term in the analytical compatibility constraint, but exact correspondence can only be obtained using the discrete compatibility constraint, yielding a solution that only differs from the exact solution because of discretization errors. Values for the velocity, exceeding the axis: $u = 10.6$ m/s (top left), $u = 4.1$ m/s (top right), $u = 33.4$ m/s (bottom left), $u = 3.7$ m/s (bottom right).

The solutions for both methods in case of pure convection after 1 and 10 s are shown in Fig. 15. When using a damping factor $\zeta = 0.5$, as in the low-order simulation, results could not be retained stable. Hence, we took $\zeta = 0.1$ (For stability at this time step size: $\zeta < 0.17$ is required.)

The profiles of density and mass weighted mixture fraction show little differences, due to the very small time step. So, if the time step is taken small enough, both methods yield almost identical results. The only meaningful difference is noticeable at the left step, where monotonicity is not preserved, using the analytical compatibility-constraint pressure-correction method. This is an artefact due to the inexact correspondence with the equation of state. A discussion on the results for velocity is more subtle, as explained now.

Because the two methods considered both impose the equation of state (in a weak or hard way), they behave very similarly. The 1D purely convective test case is the simplest case to show and to analyse this behavior. Because of the numerical discretization the initial sharpness of the front is not retained, creating a numerical reaction zone. The reaction results in a flow acceleration. Thus, the velocity field immediately reacts to numerical errors at the front's position. Both methods show this behavior. The equation of state is only approximately fulfilled in case of the analytical constraint with penalty term, whereas the fulfillment is exact with the discrete compatibility constraint. A result hereof for both methods is the instantaneous deviation of the velocity field, for which the error is strongly related to the numerical discretization of the convective terms (first order upwind, second order TVD,...). Note that this velocity error is of much less importance if there is a physical diffusion, as is mostly the case.

It can be noticed from Fig. 15 that there is a strong deviation from the exact analytical solution (a constant velocity field). Among all variables, the velocity field is the most challenging field to predict correctly. This is due to the fact that in a 1D flow, the velocity field does not follow from an evolution equation in time. Hence, there is no smoothing effect from the time-stepping procedure. The velocity field immediately reacts to the approximate (and thus incorrect) prediction of the variables density and mixture fraction and is hence extremely sensitive to the numerical error at a certain instant in time. We do want to stress the fact that both the analytical compatibility-constraint method with penalty term and the discrete

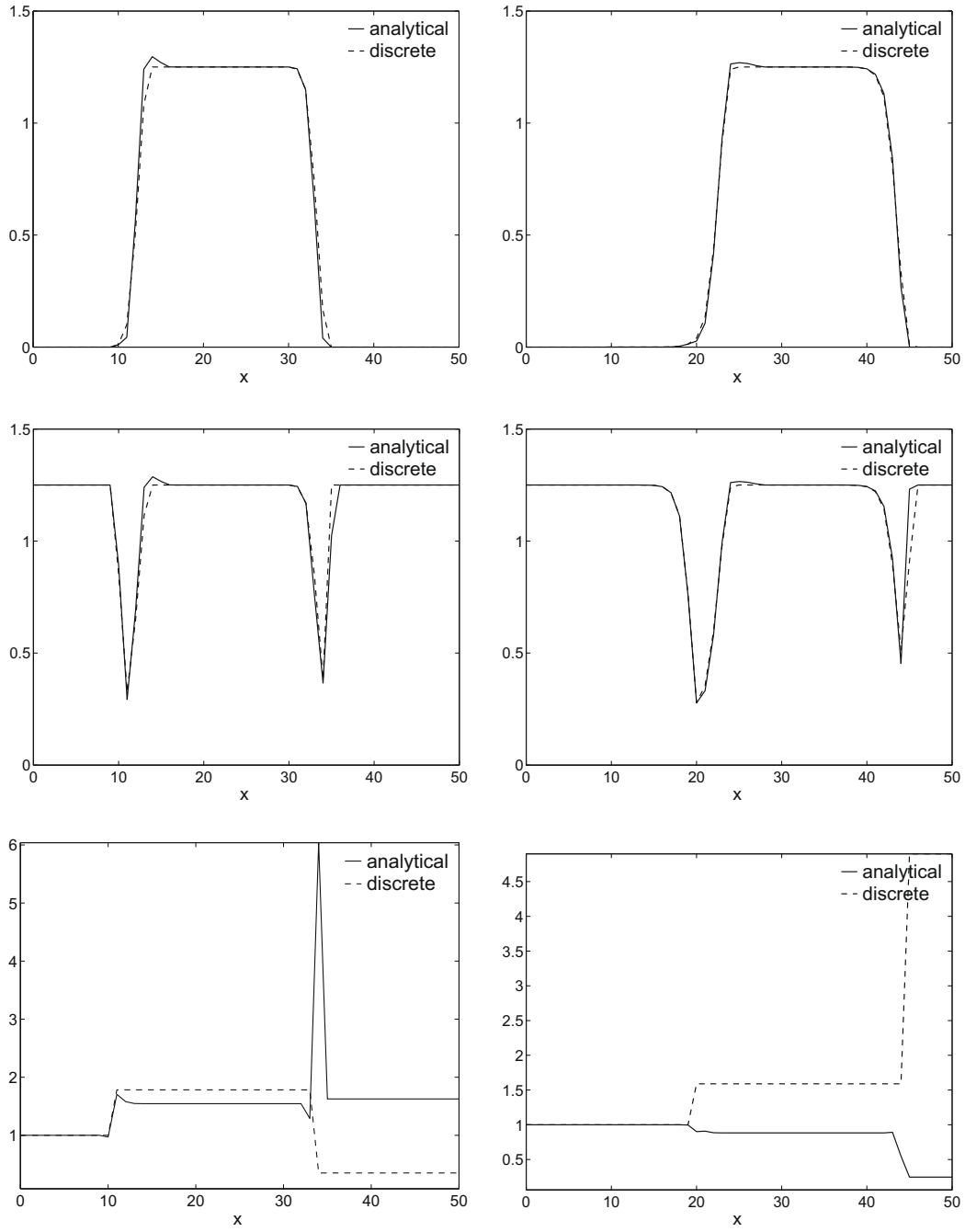

Fig. 15. Mass weighted mixture fraction (top), density (center) and velocity (bottom) fields, obtained with the analytical compatibility-constraint with damping factor $\zeta = 0.1$ (anal.) and the discrete compatibility constraint (discr.) pressure-correction algorithm after 1 (left) and 10 (right) seconds for pure convection of reacting fluids. Apart from the non-monotonicity in case of the analytical scheme, both schemes yield identically good results for ρ and $\rho\xi$-fields. Comparison between instantaneous velocity fields is not meaningful, since they oscillate in time.

compatibility-constraint method suffer from this sensitivity. Nevertheless, they are the only valid options if one wishes to accurately simulate a non-premixed combustion case (cf. 2D examples).

From the above reasoning, it is clear that a depicted velocity field at a certain instant in time is not meaningful in case of a 1D purely convective problem because it responds immediately to numerical errors. The resulting velocity at a certain grid point oscillates in time. This oscillating behavior is enhanced if a numerical discretization is chosen that keeps the fronts as sharp as possible, e.g. a TVD scheme with superbee limiter. To that purpose, this limiter acts diffusive and/or anti-diffusive, depending on the front's shape and position. The resulting velocity errors oscillate in time: sometimes the errors are positive,

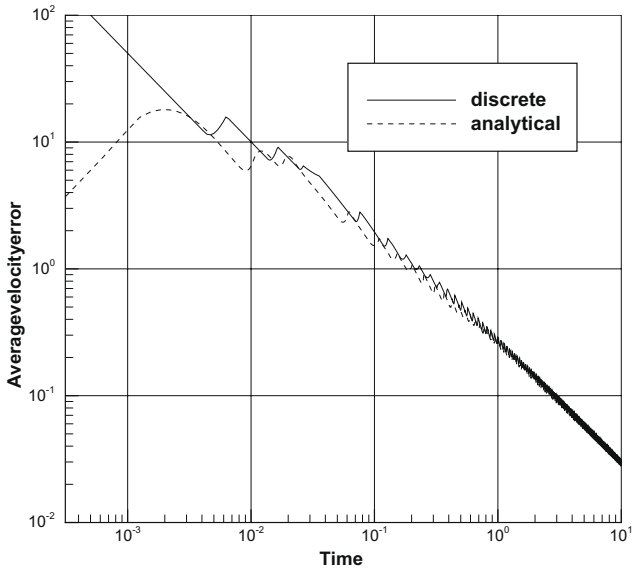

Fig. 16. Time-averaged outlet velocity error as a function of simulated time, obtained with the higher order discrete compatibility-constraint pressure-correction algorithm (—) and the analytical compatibility-constraint pressure-correction algorithm with damping factor $\zeta = 0.1$ (– –) on a grid with grid spacing $\Delta x = 1/16$ m.

sometimes they are negative. To assess the accuracy of the method, we do wish to incorporate this velocity field, since it is the velocity that deviates the most from the exact solution. Even more, since the flow is one-dimensional and the velocity is fixed at the inlet, all errors accumulate at the outlet. Therefore, the highest error is seen in the value of the velocity at the outlet. To assess the accuracy of the methods, we therefore focus on the prediction of this velocity-value as a function of simulated time. To alleviate the oscillating behavior, the time-averaged error for the outlet velocity is depicted in Fig. 16. If this error approximates zero, the front moves at the correct speed and the average outlet velocity is well predicted.

Fig. 16 tells more than just one simulation on one grid. Since, for the convective test-case, no absolute length scale exists, there is a one-to-one relation between simulated time and grid refinement. A solution obtained at a longer simulated time corresponds to a finer grid solution. As long as the two fronts do not interfere, the only non-dimensional parameter is the CFL-number, relating the time step (Δt) and the grid spacing (Δx):

$$CFL = u_{inlet}\frac{\Delta t}{\Delta x}.$$

For a reference grid with grid spacing Δx_{ref}, the result after t_{ref} seconds is obtained using n_{ref} time steps:

$$t_{ref} = n_{ref}\Delta t_{ref}.$$

The result at the same simulated time on a different grid, with the same, constant CFL, can be found after n_1 time steps with $t_{ref} = n_1\Delta t_1$ and thus:

$$\frac{n_1}{n_{ref}} = \frac{\Delta t_{ref}}{\Delta t_1} = \frac{\Delta x_{ref}}{\Delta x_1}.$$

As such, the $u_{out}(t)$-plot for the discrete compatibility-constraint pressure-correction method shows the convergence of the method as the grid becomes finer, with $t = n\Delta t_{ref} = t_{ref}\Delta x_{ref}/\Delta x$.

Fig. 17 shows the results for the purely diffusive test case, obtained with a second order TVD scheme with superbee limiter. Since no analytical solution exists for this case, a reference (grid-converged) result on a finer grid is shown for comparison. In the purely diffusive test case, again, the velocity at the outlet is the most challenging prediction, but, as already mentioned, it is governed by physical diffusion and hence has a more regular behavior.

In contrast to the purely convective test case, this case now has a distinct time and length scale. Hence, a grid-refinement in the pure sense can be performed. This is done (Fig. 18) for grids with a spacing down to $\Delta x = 1/16$ m. Due to numerical artefacts (discretization), the velocity field again oscillates in time, but converges as grids become finer.

6. Two-dimensional mixing layer

6.1. Problem description

A second test case is a laminar mixing layer. Two different fluids enter separately at the same speed into a straight channel, where mixing takes place. Note that no experimental data are available for this purely numerical test case.

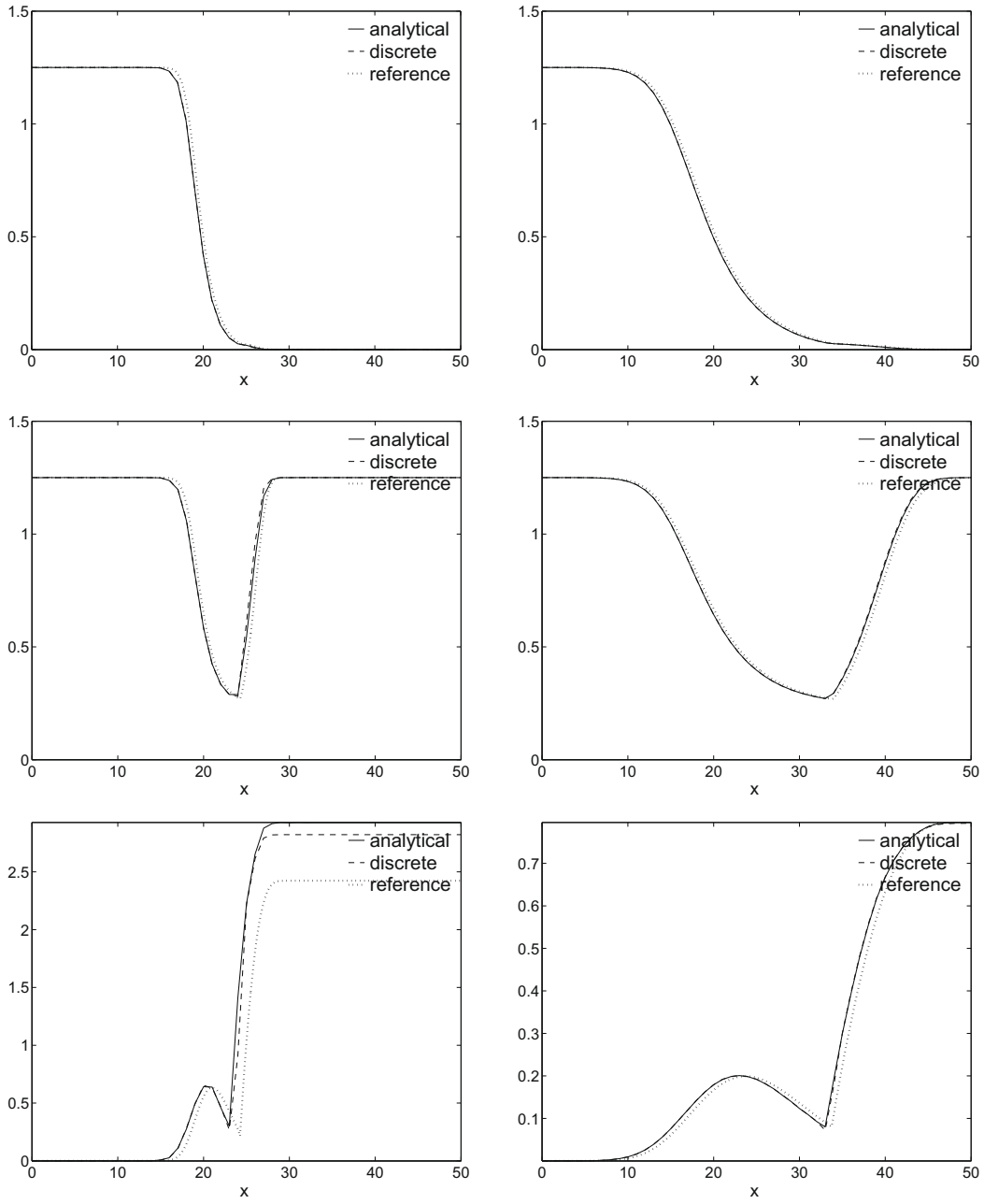

Fig. 17. Mass weighted mixture fraction (top), density (center) and velocity (bottom) fields, obtained with the analytical compatibility-constraint with damping factor $\zeta = 0.1$ (anal.) and the discrete compatibility constraint (discr.) pressure-correction algorithm after 1 (left) and 10 (right) seconds for pure diffusion of reacting fluids. The methods show little differences.

The emphasis in this section is not on an accurate prediction of the test case, but on the stability of the algorithms when applied in different situations. Therefore, different time-accurate calculations of the test case are performed with increasing time steps, kept constant during the simulation.

A 32×16 colocated vertex-centered mesh of 1 m $\times$ 0.5 m is used, with square cells. The upper and lower boundary are walls. The two fluids (fluid A and B in case of inert mixing, or Fuel and Oxidizer, representing non-premixed combustion (see Fig. 19)) enter at the left boundary and leave the domain on the right. The mixing process is described by the mixture–fraction equation. The equation of state, imposing the density mixture–fraction relationship, is Eq. (33) for inert mixing or Eq. (34) non-premixed combustion.

The fluid's viscosity is set to 0, but species diffusion is admitted with a species diffusivity equal to $\rho D = 0.015625$ Pa s. Note that, because of the hypothetical nature of the test case, this value is arbitrary and is chosen in a way that a nicely

rithm is used, a similar correction is added to the mass flux at the cell faces [17].

6.3. Results

6.3.1. Inert mixing layer

A density ratio of 10 is applied at the inlet of the domain ($\rho_A = 1$ kg/m^3; $\rho_B = 0.1$ kg/m^3). The density ratio is maximal at the inlet of the domain. The maximum time step that yields a stable simulation in the inert-mixing case is reported in Table 2.

Table 2
Maximum allowable time step (in s) for stability during the simulation of the 2D inert mixing layer. The different pressure-correction schemes are comparable with respect to stability.

Continuity-constraint	Compatibility-constraint
0.00014	0.0001

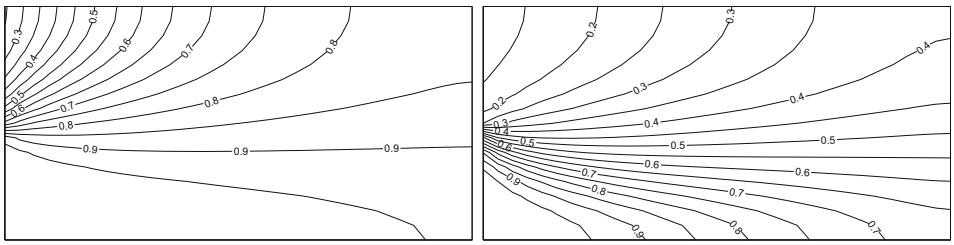

Fig. 20. Converged solution of the 2D inert mixing layer: contourlines of mixture fraction (left) and density (right). The result is independent of the pressure-correction scheme.

Table 3
Maximum allowable time step (in s) to obtain a stable steady-state solution during the simulation of the 2D reacting mixing layer. The continuity-constraint pressure-correction scheme does not yield stable results, unless a rescaling of the density time derivative is used with rescaling factor α. The drift from the equation of state is controlled in the analytical continuity-constraint scheme, using a damping factor ζ.

Continuity-constraint		Analytical compatibility-constraint		Discrete compatibility-constraint
Δt	α	Δt	ζ	Δt
–	1	0.00016	0	0.00022
0.00004	0.1	0.00017	0.1	
0.00006	0.01			

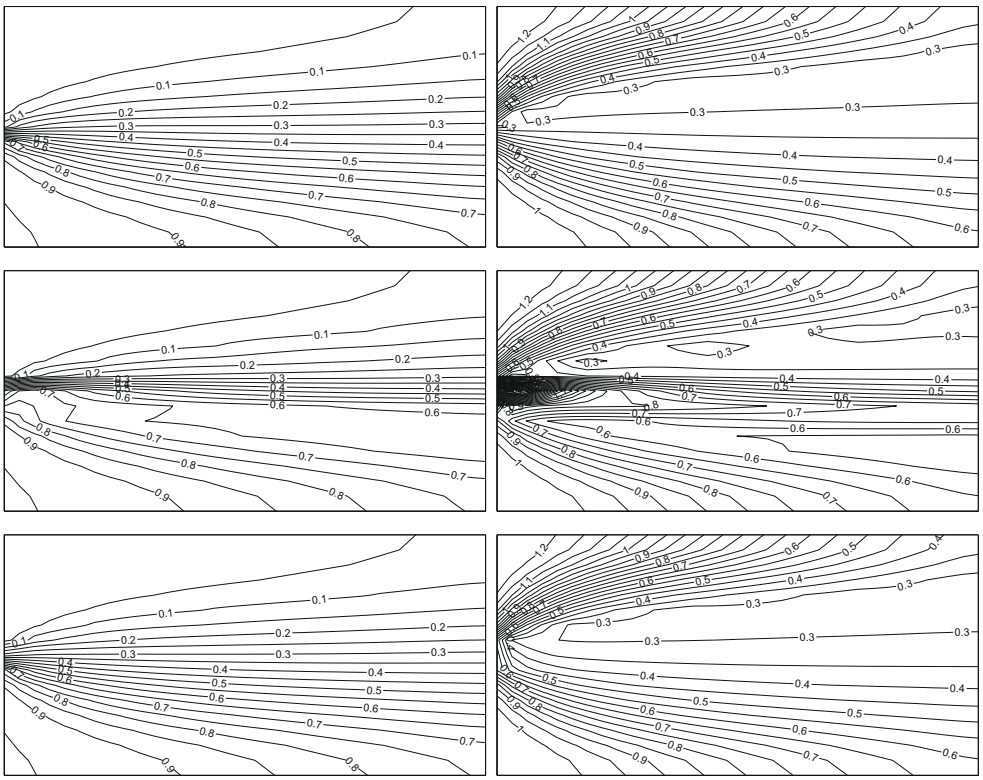

Fig. 21. Converged solution of the 2D reacting mixing layer, obtained with the continuity-constraint or the discrete compatibility-constraint (top), with the analytical compatibility constraint pressure-correction scheme without penalty term (center) and with damping factor $\zeta = 0.1$ in the penalty term (bottom): contourlines of mixture fraction (left) and density (right).

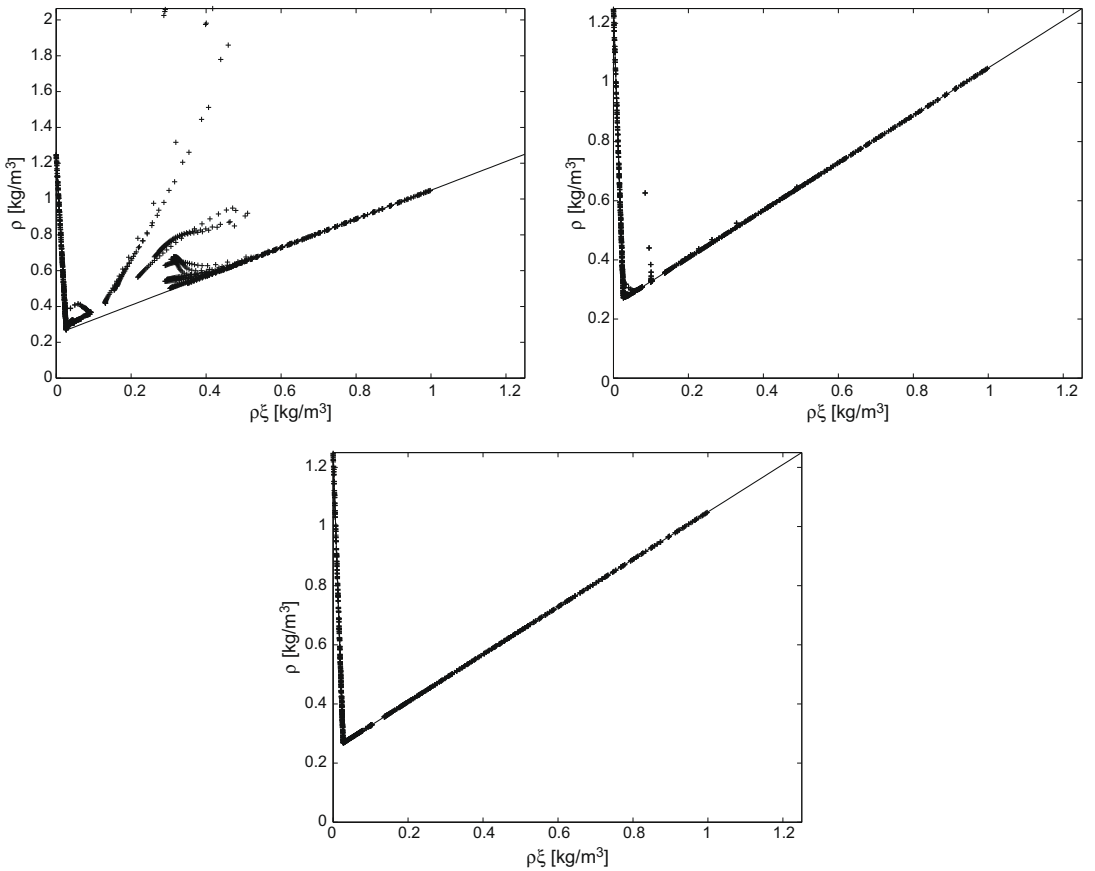

Fig. 22. Scatter plot of the obtained density and fuel elements density predictions in the converged solution of the 2D reacting mixing layer, obtained with the analytical compatibility-constraint pressure-correction scheme without penalty term (top left), with damping factor $\zeta = 0.1$ in the penalty term (top right) and with the discrete compatibility-constraint pressure-correction method (bottom): even in the converged solution, the equation of state is not fulfilled in case of an analytical compatibility-constraint. The drift is ameliorated with the introduction of a penalty term, but only the discrete compatibility-constraint predicts states that match the equation of state in an exact manner.

Table 4
Number of iterations of Newton's method needed during the first 1000 time steps of the discrete compatibility-constraint pressure-correction scheme with $\Delta t = 0.0002$ s: in most cases, only one iteration is sufficient.

Number of iterations	Occurrences	Frequency (%)
7	2	0.2
6	5	0.5
5	5	0.5
4	5	0.5
3	27	2.7
2	123	12.3
1	833	83.3

We conclude that all pressure-correction algorithms[1] yield a stability limit that is of the same order of magnitude. This is not surprising: also in the 1D tests involving inert mixing, a relatively good prediction was obtained, especially in case of purely diffusive transport (Fig. 10, top). In case of pure convection (Fig. 3, top), the simulation results became unstable, but inaccuracies were restricted to the region close to sharp gradients. Including diffusion alleviates the convective inaccuracy.

From Table 2, the conclusion must not be drawn that the continuity-constraint pressure-correction scheme is more stable than the compatibility-constraint pressure-correction because the maximum allowable time step is slightly larger. Indeed, because a different algorithm is used, different results for e.g. velocity are obtained during time stepping. Since the

[1] Recall that in case of inert mixing, the discrete and analytical compatibility-constraint pressure-correction schemes are identical.

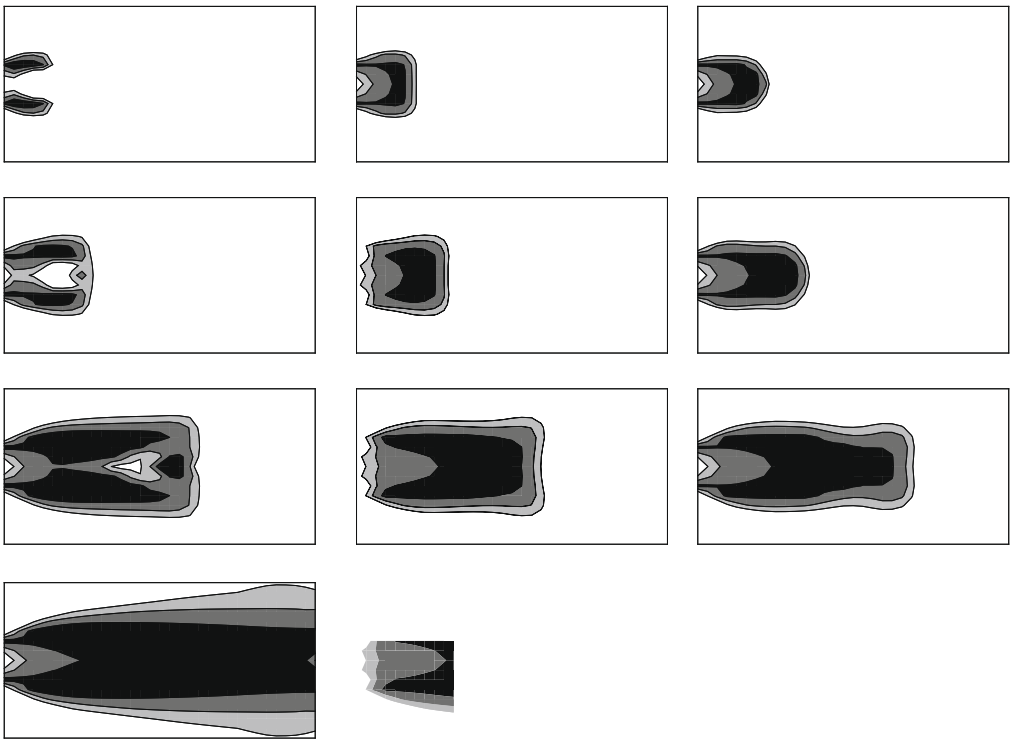

magnitude of velocity has a direct impact on the maximum time step for stability through the CFL-number, the reported maximum time step is also influenced by this.

The converged solution is independent of the pressure-correction scheme and is depicted in Fig. 20.

6.3.2. Reacting mixing layer

Since the density of pure Fuel and pure Oxidizer are assumed equal ($\rho_F = \rho_O = 1.25$), there is no density ratio between the incoming fluxes at the inlet. Due to chemical reaction, large density ratios appear inside the domain. No stable results could be obtained for the reacting test case, using the continuity-constrained scheme, unless the density time derivative in the continuity equation is rescaled by a factor $\alpha < 1$:

$$\frac{\partial \rho u_i'}{\partial x_i} = -\frac{\partial \rho u_i^*}{\partial x_i} - \alpha \frac{\partial \rho}{\partial t}.$$

Note that this corrupts time accuracy. The maximum time step is given as a function of α in Table 3. The maximum time step in reacting flows is smaller than for the non-reacting case, due to the higher velocity magnitudes, caused by flow acceleration. For the continuity-constraint scheme to be stable in reacting flows, not only the use of a rescaling factor is necessary, but also a remarkably smaller time step has to be used, compared to the discrete compatibility-constraint scheme.

For the time steps, listed in Table 3, the same converged solution was obtained with the continuity-constraint pressure-correction scheme and the discrete compatibility-constraint pressure-correction scheme. A contourplot of the converged solution is depicted in Fig. 21 (top).

However, and remarkably, a different steady-state is obtained when the analytical compatibility-constraint pressure-correction scheme is used (Fig. 21, center). This stems from the uncontrolled drift from the equation of state (Fig. 22, top left). The equation of state is indeed not imposed in a hard manner but in a weak sense, through the material derivative.

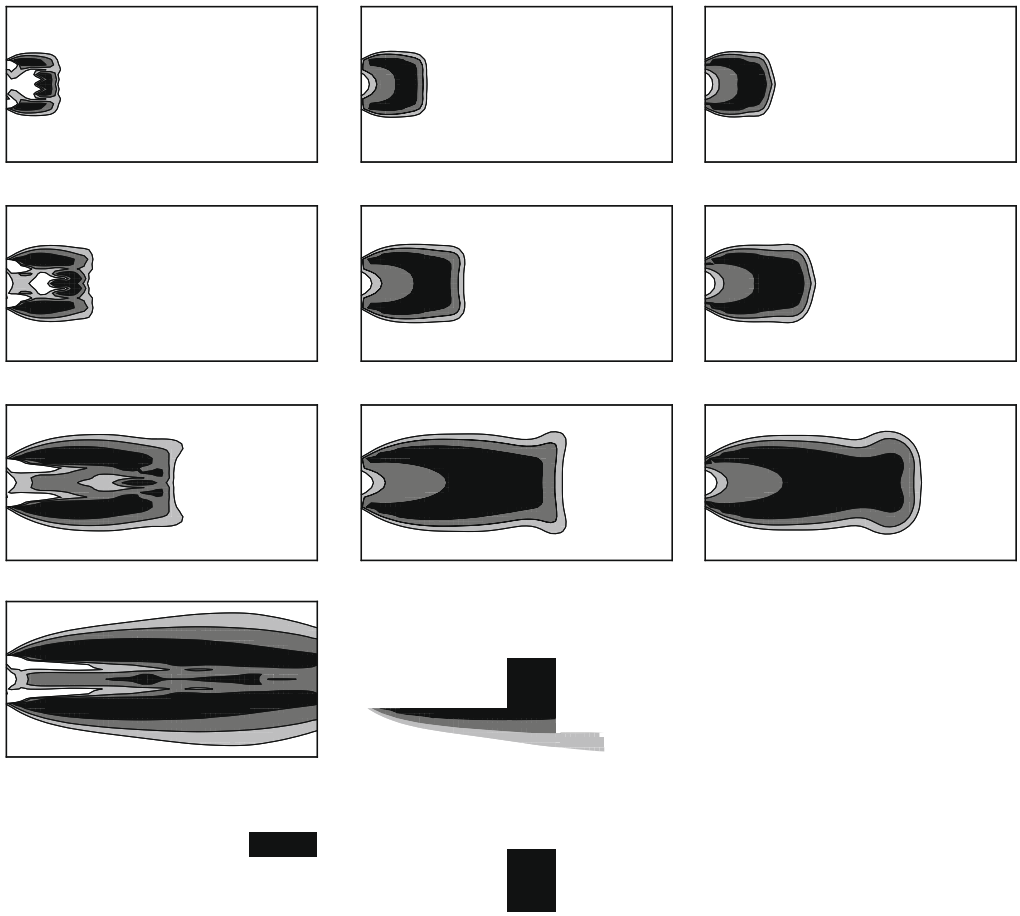

The drift from the equation of state can be controlled, using a penalty term. Here, the value for the damping factor was taken as $\zeta = 0.1$. This results yet in a different converged solution, as depicted in Fig. 21 (bottom), since the obtained states are closer to the equation of state (Fig. 22, top right). Still, in some nodes, large errors remain. Also note that, in practice, it is not straightforward to choose ζ.

Using the discrete compatibility-constraint pressure-correction-scheme yields, by definition, density and fuel elements density fields that correspond exactly to the equation of state (Fig. 22, bottom). There is, as earlier mentioned, a price to pay: the equation for pressure is a non-linear equation and requires several iterations of Newton's method per time step, inducing an extra computational cost. From the 1D test cases, we concluded that at most two iterations were needed per time step. In two dimensions, this statement no longer holds. However, if we monitor the actual amount of iterations of Newton's method needed during the time stepping of this test case (Table 4), we can conclude that the extra cost involved, remains very low for more general 2D test cases. Mostly only one iteration is needed and the maximum number of iterations (7) is only encountered in two time steps out of 1000. The extra cost is thus marginal compared to the benefits associated with this algorithm (including the higher time step limit).

7. Two-dimensional transient flame simulation

In order to assess the potential of the new pressure-correction method for transient flow calculations, a 2D test-case for combusting flow is set up. We used the same values for the physical properties as in the case of the reacting mixing layer of Section 6.3.2. Fuel enters centrally over a section of 9.375×10^{-2} m, which spans 3 grid cells of the coarsest grid, at a speed $v = 0.433$ m/s in a confined domain of width 0.5 m and length 1 m. Over the remainder of the section, air enters at a speed

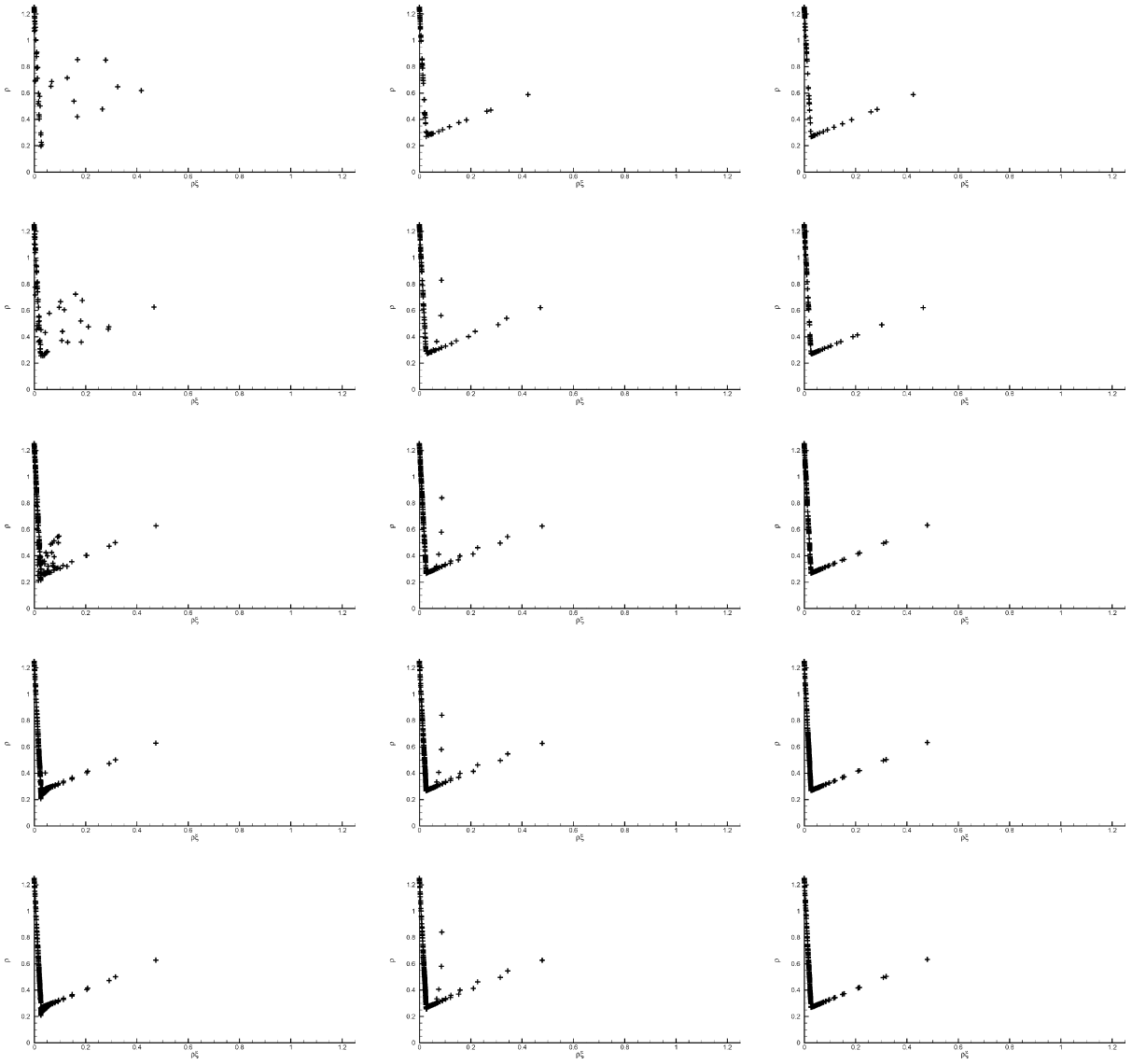

Fig. 25. Time evolving state plots. Solutions are shown for simulations on a coarse mesh (32×16) for the analytical compatibility-constraint pressure-correction method with $\zeta = 0$ (left), for the analytical compatibility-constraint pressure-correction method with $\zeta = 0.1$ (centre) and for the discrete compatibility-constraint pressure-correction method (right) at times $t = 0.006$ s,$t = 0.01$ s,$t = 0.02$ s,$t = 0.04$ s and $t = 0.08$ s (convergence).

$v = 1$ m/s. At time $t = 0$, the central inlet stream switches from air to fuel, with equal velocity, after which a flame develops. The flame can be visualized by regions of high temperature, or, with $T = p_0/\rho$, regions of low density. The simulation is performed on two different grids (coarse: 32×16 grid cells ($\Delta t = 2.10^{-4}$ s); fine: 64×32 grid cells ($\Delta t = 2.10^{-5}$ s)), using a TVD-scheme with superbee limiter for the convective terms, second order central discretization for the diffusive terms and a 4 stage low-storage Runge–Kutta Scheme for the time discretization, using both the analytical compatibility-constraint pressure-correction method, with $\zeta = 0$ and $\zeta = 0.1$, and the discrete compatibility constraint pressure-correction scheme.

A temporally evolving flame visualization for the simulations on the coarse grid is shown in Fig. 23. Initially ($t = 0.006$ s), the analytical compatibility-constraint pressure-correction scheme with penalty term acts similarly to the discrete compatibility-constraint pressure-correction scheme, whereas the analytical compatibility-constraint pressure-correction scheme without penalty term predicts an unclosed flame front in terms of temperature distribution.

At later stages, the solution obtained with the analytical compatibility-constraint pressure-correction scheme without penalty term, recovers from the wrong results in early stages and predicts a converged flame solution, comparable to the discrete compatibility scheme's prediction. The use of a penalty term causes the flame to detach from the 'burner exit'. The detached flame region is also visible in the state plots (Fig. 25), where the three states, deviating the most from the equation of state, exactly correspond to the fuel/air interface near the inlet. Also note that the analytical compatibility-constraint pressure-correction scheme without penalty term predicts temperatures, that are higher than physically possible.

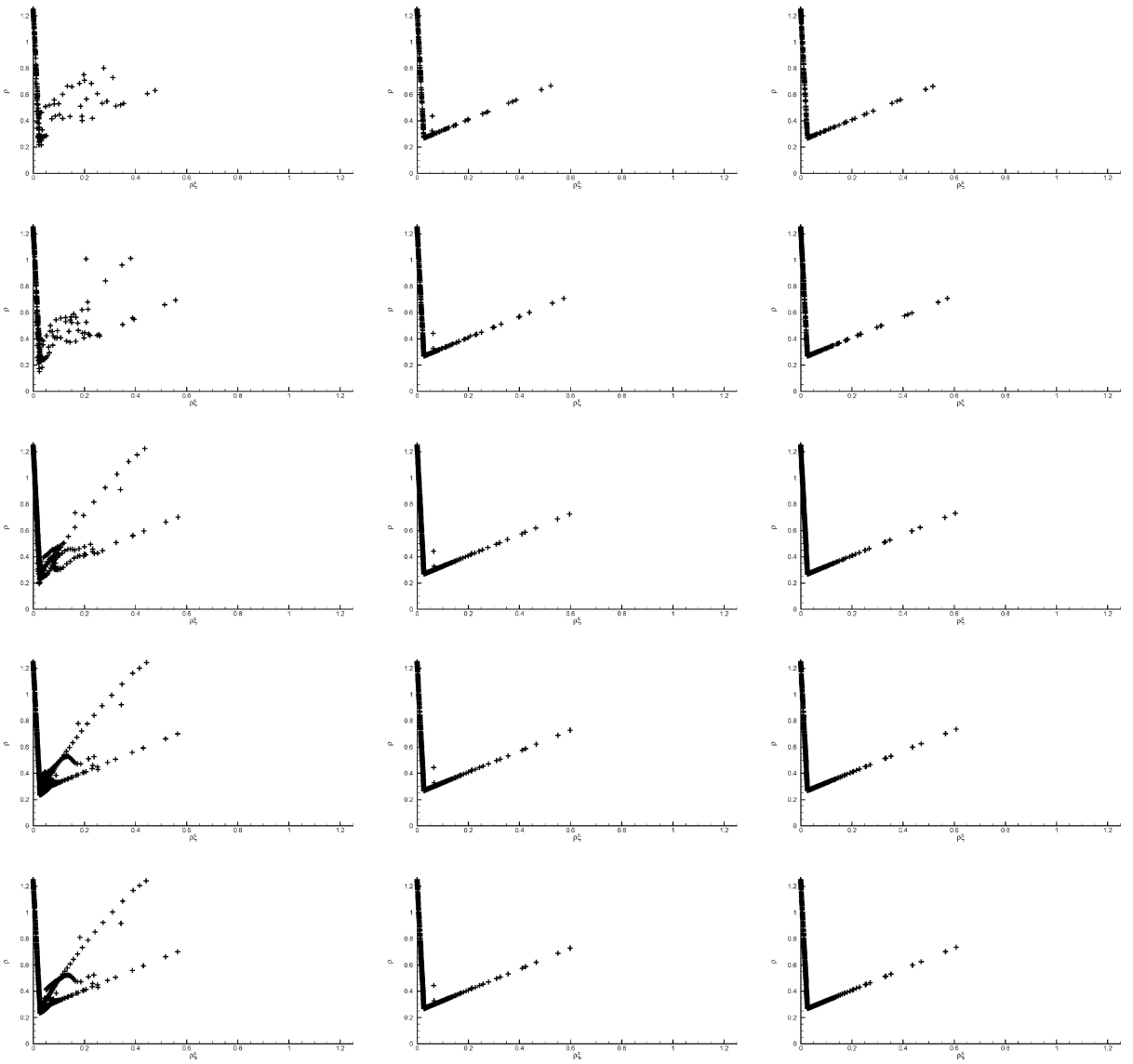

Fig. 26. Time evolving state plots. Solutions are shown for simulations on a finer mesh (64×32) for the analytical compatibility-constraint pressure-correction method with $\zeta = 0$ (left), for the analytical compatibility-constraint pressure-correction method with $\zeta = 0.1$ (centre) and for the discrete compatibility-constraint pressure-correction method (right) at times $t = 0.006$ s,$t = 0.01$ s,$t = 0.02$ s,$t = 0.04$ s and $t = 0.08$ s (convergence).

When refining the grid, the discrete compatibility-constraint pressure-correction scheme qualitatively predicts the same result (Fig. 24). The analytical compatibility-constraint pressure-correction scheme without penalty term now predicts a solution that is totally wrong, as can also be noticed from the state plots (Fig. 26). The analytical compatibility-constraint pressure-correction scheme with penalty term predicts a solution that is closer to reality: the flame is still detached, but now over a significantly smaller region. The deviations from the equation of state also become smaller. This conclusion is consistent with the previous observations of Section 5.3: the smaller the time step, the smaller the difference between both methods. Interestingly, an error in the equation of state was observed at the same location in [6] for simulations with detailed chemistry.

In conclusion, this test case shows the importance to exactly fulfill the equation of state, in order to obtain physically plausible results and to avoid false solutions.

8. Conclusions

In this paper, we developed the discrete compatibility-constraint pressure-correction algorithm for transient simulations of variable density flows at low-Mach numbers. The constraint for the velocity field is constructed from a combination of the

discrete equations of continuity and scalar transport, imposing that the newly predicted state must be compatible, in agreement with the equation of state. This way, mass and scalar conservation are guaranteed and the equation of state is exactly fulfilled at every time step.

The algorithm was tested in three example fluid configurations: a single-fluid ideal gas, a two-fluid inert mixture and a two-fluid combusting mixture. The latter is special in the sense that the equation of state is not everywhere differentiable. For comparison, two types of well-known pressure-correction algorithms were used.

From the application to several one and two-dimensional test cases, involving sharp density gradients, we conclude that the continuity-constraint pressure-correction algorithm must not be applied when sharp density gradients appear, due to lack of stability. Only when there is a considerable amount of diffusion and if the equation of state is linear, a stable result can be obtained. However, in case of reacting flows, the simulation cannot be stabilised. Possible measures to cure the stability corrupt time-accuracy, which jeopardises use in transient simulations. The analytical compatibility-constraint pressure-correction algorithm performs better with respect to stability. In case of combusting flow simulation, however, inaccurate solutions are obtained and states are predicted that deviate strongly from the equation of state. The use of a penalty term in the constraining equation, driving the solution closer to the exact equation of state, ameliorates the results. However, a careful choice of the damping factor ζ is needed, which has to be tuned in a problem dependent manner.

The newly developed algorithm performs well on all test cases. Stable results are obtained, that exactly match the equation of state, with only a minimal additional computational effort.

References

[1] J.B. Bell, D.L. Marcus, A second order projection method for variable density flows, J. Comput. Phys. 101 (1992) 334–348.
[2] H. Bijl, P. Wesseling, A unified method for computing incompressible and compressible flows in boundary-fitted coordinates, J. Comput. Phys. 141 (1998) 153–173.
[3] A.J. Chorin, Numerical solution of the Navier–Stokes equations, Math. Comput. 22 (1968) 745–762.
[4] A.J. Chorin, On the convergence of discrete approximations to the Navier-Stokes equations, Math. Comput. 23 (1969) 342–353.
[5] A.W. Cook, J.J. Riley, Direct numerical simulation of a turbulent reactive plume on a parallel computer, J. Comput. Phys. 129 (1996) 263–283.
[6] M.S. Day, J.B. Bell, Numerical simulation of laminar reacting flows with complex chemistry, Comb. Theory Model. 4 (2000) 535–556.
[7] K.C. Karki, S.V. Patankar, Pressure based calculation procedure for viscous flows at all speeds in arbitrary configurations, AIAA J. 27 (9) (1989) 1167–1174.
[8] S. Klainerman, A.J. Majda, Compressible and incompressible fluids, Commun. Pure Appl. Math. 35 (1982) 629–651.
[9] R. Klein, Semi-implicit extension of a Godunov-type scheme based on low Mach number asymptotics 1: one-dimensional flow, J. Comput. Phys. 121 (1995) 213–237.